

# Outer Van Allen radiation belt response to interacting interplanetary coronal mass ejections

E.K.J. Kilpua<sup>1</sup>, D.L. Turner<sup>2</sup>, A. Jaynes<sup>3</sup>, H. Hietala<sup>4,5</sup>, H.E.J. Koskinen<sup>1</sup>, A. Osmane<sup>1,6,7</sup>, M. Palmroth<sup>1,8</sup>, T.I. Pulkkinen<sup>9</sup>, R. Vainio<sup>4</sup>, D. Baker<sup>10</sup>, S. Claudepierre<sup>2</sup>

<sup>1</sup>Department of Physics, University of Helsinki, Helsinki, Finland

<sup>2</sup>The Aerospace Corporation, El Segundo, CA USA

<sup>3</sup>Physics and Astronomy, University of Iowa

<sup>4</sup>Department of Physics and Astronomy, University of Turku, Turku, Finland

<sup>5</sup>Department of Earth, Planetary, and Space Sciences, University of California, Los Angeles, CA, USA

<sup>6</sup>Rudolf Peierls Centre for Theoretical Physics, University of Oxford, UK

<sup>7</sup>School of Electrical Engineering, Aalto University, Espoo, Finland

<sup>8</sup>Finnish Meteorological Institute, Helsinki, Finland

<sup>9</sup>Department of Climate and Space Science and Engineering, University of Michigan, Ann Arbor, MI, USA

<sup>10</sup>Laboratory for Atmospheric and Space Sciences, University of Colorado, Boulder, CO, USA

## Key Points:

- Detailed response of the outer belt to substructures in a complex solar wind driver investigated
- Most substructures in the interacting ICMEs here deplete the core radiation belt population, but inject source electrons
- Core electrons enhanced during sustained chorus and Pc5 activity and lack of losses

---

Corresponding author: Emilia Kilpua, [emilia.kilpua@helsinki.fi](mailto:emilia.kilpua@helsinki.fi)

## Abstract

We study the response of the outer Van Allen radiation belt during an intense magnetic storm on February 15-22, 2014. Four interplanetary coronal mass ejections (ICMEs) arrived at Earth, of which the three last ones were interacting. Using data from the Van Allen Probes, we report the first detailed investigation of electron fluxes from source (tens of keV) to core (MeV) energies and possible loss and acceleration mechanisms as a response to substructures (shock, sheath and ejecta, and regions of shock-compressed ejecta) in multiple interacting ICMEs. After an initial enhancement induced by a shock compression of the magnetosphere, core fluxes strongly depleted and stayed low for four days. This sustained depletion can be related to a sequence of ICME substructures and their conditions that influenced the Earth's magnetosphere. In particular, the main depletions occurred during a high-dynamic pressure sheath and shock-compressed southward ejecta fields. These structures compressed/eroded the magnetopause close to geostationary orbit and induced intense and diverse wave activity in the inner magnetosphere (ULF Pc5, EMIC and hiss) facilitating both effective magnetopause shadowing and precipitation losses. Seed and source electrons in turn experienced stronger variations throughout the studied interval. The core fluxes recovered during the last ICME that made a glancing blow to Earth. This period was characterized by a concurrent lack of losses and sustained acceleration by chorus and Pc5 waves. Our study highlights that the seemingly complex behavior of the outer belt during interacting ICMEs can be understood by the knowledge of electron dynamics during different substructures.

## 1 Introduction

The outer Van Allen belt [e.g., *Van Allen*, 1981] is a region of high-energy electrons that are trapped in the Earth's magnetic field, encircling our planet at distances from about 3 to 7 Earth radii ( $R_E$ ). Electron fluxes in the belt are highly variable, in particular during geomagnetic storms when drastic changes occur in time scales from minutes to days [e.g., *Reeves et al.*, 2003; *Baker et al.*, 2014; *Turner et al.*, 2014]. The mechanisms that govern electron dynamics are fundamental plasma physical processes that occur in many space and astrophysical environments. There is also a significant interest to forecast the variations of the outer belt for space weather purposes; high-energy electrons in the belts pose a significant threat for the increasing number of satellites that pass through this region [e.g., *O'Brien*, 2009; *Green et al.*, 2017]. Our understanding of the radiation belts has been revolutionized during the past few years owing to the data from NASA's Van Allen Probes [*Mauk et al.*, 2013] launched in August 2012. In particular, this twin satellite mission has added significant new information on the variability of the belts as a function of energy and distance from Earth [e.g., *Baker et al.*, 2013a; *Reeves et al.*, 2013; *Thorne et al.*, 2013; *Turner et al.*, 2015; *Reeves et al.*, 2016].

Electrons in the outer belt are usually divided to source (a few tens of keV), seed (a few hundreds of keV) and core (MeV) populations. While orbiting the Earth, these electrons move in variable geomagnetic field conditions and through regions populated by various plasma waves that can lead to their acceleration, transport and scattering [see, e.g. *Baker et al.*, 2018; *Artemyev et al.*, 2014; *Osmane et al.*, 2016; *Artemyev et al.*, 2016, and references therein]. The overall response of the electron fluxes is thus dictated by several competing processes, and as emphasized, e.g., by *Summers et al.* [2007], some wave modes can cause both acceleration and scattering depending on the electron energy and when and where the electrons encounter the wave.

The electrons are lost either by encountering the dayside magnetopause (magnetopause shadowing) or by precipitating into the atmosphere due to pitch angle scattering. The gain in energy in turn occurs due to acceleration by local wave-particle interactions or via inward radial transport across drift shells (radial diffusion) while conserving their first adiabatic invariant.

71 Magnetopause shadowing [West *et al.*, 1972] requires that initially closed electron drift  
 72 paths intercept the dayside magnetopause. This typically occurs in the outermost part of the  
 73 belt ( $L > 4$ ), when increased solar wind dynamic pressure and/or erosion of the magne-  
 74 topause during southward interplanetary magnetic field moves the magnetopause Earth-  
 75 ward [e.g., Aubry *et al.*, 1970; Turner *et al.*, 2014] or during the main phase of a geomag-  
 76 netic storm, when the enhanced ring current weakens the Earth's magnetic field, which in  
 77 turn leads to adiabatic expansion of the electron drift shells (the so-called Dst effect) [e.g., Li  
 78 *et al.*, 1997; Kim and Chan, 1997]. The outward radial diffusion of electrons by fluctuations  
 79 in the geomagnetic field can significantly add to the magnetopause shadowing losses [e.g.,  
 80 Mann *et al.*, 2016]. The fluctuations are Pc5 Ultra Low Frequency (ULF) waves with periods  
 81 of a few minutes, or frequencies in mHz range, that resonate with the drift period of relativistic  
 82 electrons [e.g., Elkington *et al.*, 2003; Shprits *et al.*, 2008]. The Pc5 ULF waves are ubiq-  
 83 uitous in the magnetosphere and generated by various processes, such as solar wind pressure  
 84 pulses and interplanetary shocks [Kepko and Spence, 2003; Claudepierre *et al.*, 2010; Wang  
 85 *et al.*, 2017], foreshock transients [Hartinger *et al.*, 2013] and Kelvin–Helmholtz instabilities  
 86 at the flanks of the magnetopause, [Rae *et al.*, 2005; Claudepierre *et al.*, 2008; Wang *et al.*,  
 87 2017].

88 Prompt losses of highly energetic ( $\geq 2$  MeV) electrons through pitch angle scattering  
 89 are mainly attributed to their gyroresonance with electromagnetic ion cyclotron (EMIC; peri-  
 90 ods from a fraction of a second to a few seconds) waves [e.g., Meredith *et al.*, 2003; Summers  
 91 and Thorne, 2003; Usanova *et al.*, 2014; Kersten *et al.*, 2014]. These waves are generated by  
 92 anisotropic ring current proton distributions or enhanced solar wind dynamic pressure and  
 93 they are mostly observed at the duskside of the magnetosphere in the vicinity of the plasma-  
 94 sphere. Plasmaspheric hiss [e.g., Thorne *et al.*, 1973] can, in turn, scatter electrons within a  
 95 broad energy range, but the timescale of the scattering increases with electron energy, and for  
 96 relativistic electrons it ranges from one to several days [e.g., Selesnick *et al.*, 2003; Mered-  
 97 ith *et al.*, 2006]. The main source of plasmaspheric hiss is thought to be nonlinear growth  
 98 of whistler mode chorus waves as they propagate into the plasmasphere [e.g., Bortnik *et al.*,  
 99 2008; Summers *et al.*, 2014; Hartley *et al.*, 2018]. The millihertz ULF waves can also trans-  
 100 port particles radially inward, which increases their energy [e.g., Hudson *et al.*, 2008]. In  
 101 this case, electrons, however, encounter shorter magnetic field lines and lower-altitude mirror  
 102 points, and are consequently more likely to precipitate to the atmosphere [e.g., Brito *et al.*,  
 103 2012].

104 The Van Allen Probes have highlighted the importance of local wave-particle processes  
 105 by whistler mode chorus waves (from a few to a few tens of kHz) in accelerating electrons  
 106 to relativistic energies [e.g., Reeves *et al.*, 2013; Thorne *et al.*, 2013; Foster *et al.*, 2014; Li  
 107 *et al.*, 2014; Boyd *et al.*, 2018, see also Horne and Thorne [1998]]. Chorus waves are gener-  
 108 ated through the gyroresonance instability due to electrons with anisotropic distributions  
 109 injected during substorm expansion phases [e.g., Smith *et al.*, 1996; Miyoshi *et al.*, 2013]  
 110 and they are thus mostly found in the night and dawnside magnetosphere outside the plasma-  
 111 sphere. Recently, Jaynes *et al.* [2015] emphasized the role of sustained substorm injections  
 112 in producing MeV electrons; to reach the core energies source and seed electrons are pro-  
 113 gressively accelerated by chorus waves as suggested e.g. by Summers and Ma [2000] and  
 114 Meredith *et al.* [2002]. Chorus waves can, on the other hand, result in significant scatter-  
 115 ing and precipitation of electrons at lower energies [e.g., Lam *et al.*, 2010], and also lead  
 116 to micro-burst precipitation of relativistic electrons through quasi-linear or nonlinear inter-  
 117 actions during storm times [e.g., Thorne *et al.*, 2005; Artemyev *et al.*, 2016; Osmane *et al.*,  
 118 2016; Douma *et al.*, 2017].

119 As featured above, the outer radiation belt is a highly complex and variable region.  
 120 Kessel [2016] pointed out that one of the current challenges in radiation belt studies is to find  
 121 better connections of electron loss, transport and acceleration processes to different solar  
 122 wind and magnetospheric conditions.

123 The series of papers by *Hietala et al.* [2014], *Kilpua et al.* [2015a], *Turner et al.* [2015]  
 124 and [Turner et al., 2019] showed that the radiation belt response strongly depends on the  
 125 large-scale solar wind driver. In particular, *Hietala et al.* [2014] and *Kilpua et al.* [2015a]  
 126 analyzed the response during substructures related to interplanetary coronal mass ejections  
 127 [ICMEs; e.g., *Kilpua et al.*, 2017a] and stream interaction regions [SIRs; e.g., *Richardson*,  
 128 2018] using the  $> 2$ -MeV electrons at geostationary orbit. The response clearly depends  
 129 on the substructures and on the sequence they arrive at Earth. These substructures all have  
 130 distinct solar wind characteristics, and geospace responses [e.g., *Kilpua et al.*, 2017b], and  
 131 thus, also distinct response of electron fluxes is expected. As these studies used superposed  
 132 epoch analysis, they excluded complex solar wind drivers and events where multiple storms  
 133 occurred in a rapid sequence. Many storms are, however, caused by complex drivers that  
 134 consist of multiple heliospheric large-scale structures [e.g., *Zhang et al.*, 2007; *Lugaz et al.*,  
 135 2015a]. This is expected to lead to a complex and varying response of radiation belts, includ-  
 136 ing alternating periods when loss and acceleration processes dominate.

137 In this paper we make the first attempt to understand the detailed outer belt behavior  
 138 and possible loss and acceleration mechanisms caused by substructures within several inter-  
 139 acting ICMEs. We analyze a series of four ICMEs that interacted with the Earth's magne-  
 140 tosphere in February 2014 and caused an intense geomagnetic storm. We investigate how  
 141 source, seed and core populations change as a function of the  $L$ -shell during shocks, sheaths  
 142 and ejecta in this complex driver and relate these variations to solar wind conditions, level of  
 143 magnetospheric activity and prevailing magnetospheric wave activity (ULF, EMIC, hiss and  
 144 chorus).

## 145 2 Data and Methods

146 The Van Allen Probe electron flux measurements used in this paper are Level 2 data  
 147 obtained from the Magnetic Electron Ion Spectrometer (MagEIS) [*Blake et al.*, 2013] and  
 148 the Relativistic Electron Proton Telescope (REPT) [*Baker et al.*, 2013b]. We selected four  
 149 energy channels to represent the source (54 keV), seed (342 keV) and core (1547 keV and  
 150 4.2 MeV) populations. The 4.2-MeV electrons are from the REPT instrument and the oth-  
 151 ers from the MagEIS instrument. The data were then first averaged in  $L$ -shell using 0.1-  
 152 sized bins and then in time using both 6-hour and 30-minute bins. McIlwain's  $L$ -values we  
 153 use here are obtained using the external quiet OP77Q model [*Olson and Pfizter*, 1977] and  
 154 the internal International Geomagnetic Reference Field (IGRF) magnetic field model. The  
 155 data is obtained from the RBSP Science Operation and Data Center (<https://rbsp-ect.lanl.gov/science/DataDirectories.php>).  
 156

157 To analyze chorus wave activity we compiled magnetic spectral intensities using the  
 158 Van Allen Probes Magnetic Field Instrument Suite and Integrated Science (EMFISIS) [*Kletzing*  
 159 *et al.*, 2013] magnetometer Level 2 data from the EMFISIS website (<https://emfisis.physics.uiowa.edu/data/index>). We calculated the equatorial electron cyclotron fre-  
 160 quency  $f_{ce,eq}$  using the Tsyganenko and Sitnov geomagnetic field model (TS04D) [*Tsygan-*  
 161 *enko and Sitnov*, 2005]. The lower band chorus waves are commonly considered to be lo-  
 162 cated between  $0.1f_{ce,eq} < f < 0.5f_{ce,eq}$  and the upper band between  $0.5f_{ce,eq} < f <$   
 163  $1.0f_{ce,eq}$ . However, at higher latitudes significant chorus wave power may be observed at  
 164 frequencies below  $0.1f_{ce,eq}$ , typically identified as patches that continue from the main cho-  
 165 rus range downwards [e.g., see examples from *Cattell et al.*, 2015; *Xiao et al.*, 2017]. The  
 166 hiss waves occur above about 100 Hz and below  $\sim 0.1f_{ce,eq}$  inside the plasmasphere and  
 167 typically from evening to midnight and morning sector [e.g., *Hartley et al.*, 2018]. We have  
 168 calculated here the hiss power using the range from 100 Hz to  $0.9f_{ce,eq}$ . The density to esti-  
 169 mate whether the Van Allen Probes are inside or outside the plasmasphere is obtained from  
 170 the EMFISIS L4 data.  
 171

172 The ULF and EMIC wave powers were calculated using the geostationary GOES-13  
 173 and GOES-15 spacecraft magnetometer [*Singer et al.*, 1996] 0.512-second magnetic field

190 **Table 1.** Strong activity thresholds for different wave powers investigated in this study. The thresholds were  
 191 defined as ten times the quiet time levels using averages over the interval from 3 to 15 UT on February 17,  
 192 2014.

Wave	Strong Activity Threshold
lower band chorus	$1.3 \times 10^{-8} \text{ nT}^2 \text{ Hz}^{-1}$
upper band chorus	$8.1 \times 10^{-10} \text{ nT}^2 \text{ Hz}^{-1}$
hiss	$3.5 \times 10^{-7} \text{ nT}^2 \text{ Hz}^{-1}$
ULF Pc5	$31.2 \text{ nT}^2 \text{ Hz}^{-1}$
EMIC	$0.039 \text{ nT}^2 \text{ Hz}^{-1}$

174 data obtained through <https://www.ngdc.noaa.gov/stp/satellite/goes/dataaccess.html>.  
 175 The components of the magnetic field used correspond to radial (Earthward), east-  
 176 ward and northward directions. We calculated the wavelet spectra for each component and  
 177 then summed them together to estimate the total power. From the wavelet spectrograms we  
 178 then calculated the Pc5 power by using the interval from 3 to 10 minutes (frequencies 1.6 –  
 179 5.5 mHz) and the EMIC wave power, corresponding roughly the Pc1 and Pc2 periods from 1  
 180 to 5 seconds (frequencies 0.2 – 1 Hz). We note that that geostationary GOES satellites may  
 181 not always give the completely correct picture of the EMIC wave power at the Van Allen  
 182 Probe locations [Engebretson *et al.*, 2018].

183 In the plots showing wave powers (hiss, lower and upper chorus, Pc5 and EMIC) we  
 184 indicate a threshold for "strong activity" using the ten times the quiet time levels, which were  
 185 defined using the averages over the interval from 3 to 15 UT on February 17, 2014. The  
 186 thresholds are given in Table 1. We plot the lower and upper chorus wave powers when the  
 187 density was  $< 100 \text{ cm}^{-3}$ , *i.e.*, when the Van Allen Probes were approximately outside the  
 188 plasmasphere, and the hiss power when  $n > 100 \text{ cm}^{-3}$ , *i.e.*, when the Van Allen Probes were  
 189 approximately inside the plasmasphere.

193 The times of the ICME leading and trailing edges were obtained from the Wind ICME  
 194 catalog (<https://wind.nasa.gov/ICMEindex.php>) [Nieves-Chinchilla *et al.*, 2018] and  
 195 we also checked the data for typical ICME signatures in the magnetic field magnitude, direc-  
 196 tion and variability, temperature, speed and plasma beta, etc. [see *e.g.* Kilpua *et al.*, 2017a,  
 197 and references therein]. The shock parameters were obtained from the Heliospheric Shock  
 198 Database ([ipshocks.fi](http://ipshocks.fi)) [Kilpua *et al.*, 2015b]. The subsolar magnetopause position is cal-  
 199 culated from the Shue *et al.* [1998] model, where its position depends on solar wind dynamic  
 200 pressure and IMF north-south component.

### 201 3 Results

202 Figures 1 and 2 give an overview of the entire interval (February 14–23, 2014). The  
 203 first figure shows solar wind conditions, the subsolar magnetopause position from the Shue  
 204 *et al.* [1998] model, and geomagnetic response in terms of the 1-minute AL index, which  
 205 monitors the intensity of the westward electrojet, and the 1-hour Dst index, which monitors  
 206 the intensity of the equatorial ring current [for description of geomagnetic indices see *e.g.*,  
 207 Mayaud, 1980]. The second figure shows the response of the outer radiation belt for four  
 208 selected energies representing the source (54 keV), seed (343 keV) and core (1547 keV and  
 209 4.2 MeV) populations. The panels a), c), e), and g) in Figure 2 show the  $L$  vs. time electron  
 210 spectrograms and the panels b), d), f) and h) the maximum flux for each 6-hour interval. The  
 211 corresponding  $L$ -value is indicated by gray colors.

218 **Table 2.** The times and selected parameters of the interplanetary shocks that occurred during the analyzed  
 219 events. The shock times are based on OMNI data (*i.e.*, shifted to the nose of the Earth’s bow shock) and are  
 220 taken from the Heliospheric Shock Database (`ipshocks.fi`). The columns give the shock time, magne-  
 221 tosonic Mach number ( $M_{ms}$ ), shock speed ( $V_{sh}$ ), the speed jump across the shock ( $\Delta V$ ) and the downstream  
 222 to upstream magnetic field magnitude ( $B_d/B_u$ ) ratios.

	Shock time [UT]	$M_{ms}$	$V_{sh}$ [km/s]	$\Delta V$ [km/s]	$B_d/B_u$
Shock 1	Feb 15, 13:25	2.0	469	71	2.25
Shock 2	Feb 18, 07:06	1.5	374	38	1.81
Shock 3	Feb 19, 03:56	1.9	597	91	1.39
Shock 4	Feb 20, 03:09	5.7	821	195	2.9

223 **Table 3.** The leading edge (LE) and trailing edge (TE) times of the ICME ejecta during the ana-  
 224 lyzed events. The times are according to the OMNI database and taken from the Wind ICME catalogue  
 225 (<https://wind.nasa.gov/ICMEindex.php>), considering the time shift from Wind to Earth.

	ejecta LE time [UT]	ejecta TE time [UT]
Ejecta 1	Feb 16, 04:45	Feb 16, 16:55
Ejecta 2	Feb 18, 15:45	Feb 19, 10:00
Ejecta 3	Feb 19, 12:45	Feb 20, 03:09
Ejecta 4	Feb 21, 03:15	Feb 22, 13:00

212 The shock and ICME leading and trailing edge times are marked in tables 2 and 3, in-  
 213 cluding some key shock parameters in Table 2; The magnetosonic Mach number ( $M_{ms}$ ) is  
 214 calculated as the ratio of the upstream solar wind speed in the shock frame and the magne-  
 215 tosonic speed. It describes the strength of the shock.  $V_{sh}$  is the speed of the shock,  $\Delta V$  the  
 216 speed jump across the shock and  $B_d/B_u$  the downstream to upstream magnetic field ratio  
 217 (see details from the documentation of the `ipshocks.fi`).

226 The data interval features a series of four ICMEs that all had a leading interplanetary  
 227 shock. The three last ICMEs were closely clustered, while the first ICME occurred clearly  
 228 separate from three interacting ICMEs; the trailing edge of the first ICME and the leading  
 229 shock of the second ICME were separated by about 1.5 days. We, however, included the first  
 230 ICME in the analysis, as it already changed the structure of the outer belt from typical quiet  
 231 time conditions (see below). The Dst minimum during the interval was  $-116$  nT, indicating  
 232 intense storm activity soon after the third shock (S3) impacted the Earth.

233 Before the arrival of the shock leading the first ICME, electron fluxes resemble the typ-  
 234 ical radiation belt structure during quiet conditions as depicted *e.g.*, in *Reeves et al.* [2016]  
 235 (see their Figure 7): The seed and core populations reside at relatively high  $L$ -shells with the  
 236 fluxes peaking at about  $L = 4.5 - 5$ , while the population at source energies mainly represents  
 237 the extension of the inner belt to  $L = 2 - 3.5$  (fluxes peak at the lowest  $L$ -shells). In agree-  
 238 ment with *Reeves et al.* [2016] quiet time conditions the peak of the flux in the outer belt  
 239 widens and moves toward higher  $L$ -shells with decreasing energy. The spectrogram at 4.2–  
 240 MeV energy shows some signatures of a double outer belt structure [*Baker et al.*, 2013a]:  
 241 The main population peaks at  $L = 5$ , and another, significantly fainter separate belt is located  
 242 at  $L \approx 3.5$ .

243 During the analyzed events the outer radiation belt experienced several significant vari-  
 244 ations over the time when the four ICMEs interacted with the Earth's magnetosphere. As  
 245 shown by panels e)-h) in Figure 2, the first ICME wiped out the core population in the outer  
 246 belt and the fluxes fully recovered only at the end of the investigated interval. There are,  
 247 however, some significant variations also in the core fluxes (further depletions mainly) as  
 248 the second and third ICME pass by the Earth. Source and seed population in turn experience  
 249 clearer variations. In the following subsections we will analyze in more detail the solar wind  
 250 conditions, geomagnetic response, electron flux variations in the radiation belts, and plasma  
 251 waves in the inner magnetosphere during three intervals.

### 263 3.1 Period 1: Feb 15–16, 2014

264 The interval on February 15–16, 2014 covers the first ICME, *i.e.*, shock S1, sheath  
 265 SH1 and ejecta E1. Van Allen Probes electron flux measurements are given in Figure 3 for  
 266 the same four energy channels as shown in Figure 2, but now as 30-minute averages. Figure  
 267 3 also shows the subsolar magnetopause position from the *Shue et al.* [1998] model and the  
 268 Dst and AL indices. The spectrograms featuring the chorus and hiss waves from the Van  
 269 Allen Probes and Pc5 and EMIC waves from the geostationary spacecraft GOES-13 and  
 270 GOES-15 are given in Figures 4 and 5.

294 Shock S1 had magnetosonic Mach number 2.0 and speed jump  $71 \text{ km s}^{-1}$ , which are  
 295 typical values for a shock detected near the Earth orbit [*e.g.*, *Kilpua et al.*, 2015b]. The dy-  
 296 namic pressure was high throughout sheath SH1 and the magnetopause was compressed be-  
 297 low  $9R_E$ . During ejecta E1 in turn, the dynamic pressure decreased and the magnetopause  
 298 moved back closer to its nominal position. Both sheath SH1 and ejecta E1 had dominantly  
 299 northward IMF followed by a few hours of southward field in their trailing parts. As a con-  
 300 sequence, Dst remained at quiet time levels ( $> -30 \text{ nT}$ ) throughout Period 1, but a few iso-  
 301 lated substorms occurred. A combination of northward IMF and high dynamic pressure dur-  
 302 ing sheath SH1 compressed strongly the magnetosphere and caused a several-hour period of  
 303 strongly positive Dst.

304 Notable changes occurred first only at the core energies; Soon after Shock S1, the  
 305 fluxes intensified significantly, in particular at 4.2 MeV, and the flux peak moved towards  
 306 Earth from  $L = 5$  to  $L = 4.5$ . Figure 4 shows that at this time no strong chorus or hiss ac-  
 307 tivity occurred, but according to Figure 5, the Pc5 and EMIC wave powers intensified. We  
 308 thus suggest that this initial enhancement can be largely explained by fully adiabatic inward  
 309 motion of electrons due to the compression of the Earth's magnetic field and related gain in  
 310 energy as well as a prompt acceleration by impulsive electric fields and subsequent  $\sim \text{mHz}$   
 311 ULF waves associated with the shock compressing the magnetosphere [*e.g.*, *Foster et al.*,  
 312 2015; *Kanekal et al.*, 2016] as proposed by *Su et al.* [2015] for this same interval. *Su et al.*  
 313 [2015] also reported that this interval lacked chorus waves, while ULF waves were present in  
 314 the inner magnetosphere.

315 During the end of sheath SH1, the seed and core populations depleted strongly over a  
 316 wide  $L$ -range, and the remaining flux moved even closer to Earth to  $L \simeq 3.5 - 4$  (see figures  
 317 2 and 3). This dropout and Earthward motion coincided with the magnetopause compres-  
 318 sion all the way to geostationary orbit and, as seen from Figure 4, with the intensification of  
 319 both Pc5 and EMIC power. During sheath SH1 the Van Allen Probes were predominantly  
 320 in the plasmasphere (panels 4c and 4g) and strong plasmaspheric hiss was observed. Effi-  
 321 cient losses are thus expected both due to magnetopause shadowing enhanced by the inward  
 322 electron diffusion by Pc5 fluctuations to lower  $L$ -shells [*e.g.*, *Turner et al.*, 2013] and due to  
 323 precipitation losses due to pitch angle scattering by EMIC (core electrons) and hiss waves.  
 324 After a smaller initial depletion, the source electrons, however, enhanced over a wide range  
 325 of  $L$ -shells due to substorm injections.

326 A slight enhancement of core electrons (seen at 1547 keV and in particular at 4.2 MeV)  
 327 occurred during ejecta E1. Chorus waves were observed only sporadically related to sub-

storms occurring near the boundaries of the ejecta and this enhancement could be rather related to the inward radial transport by Pc5 fluctuations. During ejecta E1, although Pc5 and EMIC wave activity subsided from the levels observed during the sheath, Pc5 power was still clearly enhanced when compared to the values before shock S1 arrival.

### 3.2 Period 2: Feb 18–19, 2014

The outer radiation belt did not experience further notable changes on February 17 (see Figure 2). The solar wind at this time was slow and undisturbed and geomagnetic activity was low. We next analyze the interval on February 18–19, 2014 covering the second and third ICMEs. The radiation belt response, chorus and ULF waves are shown in figures 6, 7, and 8 in the same format as in the previous subsection.

The second shock (S2) on February 18, at 07:06 UT was the weakest during the studied interval. The magnetosonic Mach number was 1.5 and the speed jump only  $38 \text{ km s}^{-1}$ . The magnetic field in the following sheath (SH2) was directed northward, dynamic pressure was relatively low and the magnetopause stayed far from geostationary orbit. As a consequence, this shock and sheath passed the Earth without major effects in the magnetosphere, and no significant changes occurred in the outer radiation belt electron fluxes.

Ejecta E2 had southward IMF of about  $-9 \text{ nT}$  (in GSM) causing moderate substorm activity and Dst decrease to storm levels, *i.e.*, below  $-50 \text{ nT}$ . The solar wind dynamic pressure was low and the magnetopause stayed close to its nominal position around  $10\text{--}11 R_E$ . The third shock (S3) had magnetosonic Mach number 1.9 and a speed jump  $91 \text{ km s}^{-1}$ . The shock intercepted ejecta E2 and compressed its southward field to about  $-15 \text{ nT}$ . This shock-intensified southward ejecta field drove the storm peak; Dst reached  $-116 \text{ nT}$  on Feb 19, 9 UT and caused several strong substorms (see also analysis of this event in *Lugaz et al.* [2016]). During sheath SH3 the magnetopause was beyond  $9R_E$ . As the dynamic pressure remained relatively low, the inward motion of the magnetopause as suggested by the *Shue et al.* [1998] model is mostly related to the erosion of the magnetopause due to strongly southward IMF. Ejecta E3 had in turn northward IMF and geomagnetic activity (featured both by Dst and AL) quickly subsided. Also the solar wind dynamic pressure during ejecta E3 was low, and the magnetopause stayed far from geostationary orbit.

As discussed in Section 3.1, core electron fluxes depleted strongly during the first ICME. They (both  $1547 \text{ keV}$  and  $4.2 \text{ MeV}$ ) experienced further progressive depletions during ejecta E2 and the leading part of sheath SH3 that contained the compressed ejecta E2 fields. Figure 7 shows that during the leading part of ejecta E2 Van Allen Probes were in the plasmasphere and strong plasmaspheric hiss was observed. When ejecta E2 progressed and the substorm activity started, the probes were traversing the dawnside outside the plasmasphere and strong lower band chorus power occurred. Strong chorus power (both lower and upper band) was also observed during the next dawnside orbit during sheath SH3. Figure 8 shows that the Pc5 power enhanced already during the beginning of ejecta E2, but intensified considerably a few hours before shock S3 arrived to the Earth and the activity stayed high throughout sheath SH3. The EMIC power showed similar behavior, but subsided in the trailing part of sheath SH3. We thus suggest these further depletions at core energies were associated with effective magnetopause shadowing and losses through pitch angle scattering by EMIC and hiss and possibly also by chorus waves. The magnetopause shadowing was facilitated by eroded subsolar magnetopause, radial outward transport both from non-adiabatic interactions with the ULF Pc5 fluctuations and from adiabatic Dst effect.

Source electron fluxes in turn enhanced already during the leading part of E2 when the substorm activity started, while the seed population first depleted and then considerably enhanced after shock S3, when the most intense substorm activity took place. After shock S3, the peak fluxes of source and seed populations also moved progressively to lower  $L$ -shells (from  $L \approx 5 - 5.5$  to  $L \approx 3.5 - 4$ ), consistent with substorm injections penetrating to lower  $L$ -shells with increasing activity [e.g., *Reeves et al.*, 2016]. See also *Califf et al.* [2017]



390 who showed that electrons in the range of hundreds of keV in the slot region were enhanced  
 391 at this time (also visible from panel c) of Figure 2 here). We note that core electrons also  
 392 enhanced slightly during the end part of sheath SH3, presumably due to inward Pc5 induced  
 393 transport, recovering ring current and chorus wave acceleration playing in concert.

394 During ejecta E3 no significant changes in the outer belt occurred. This is consistent  
 395 with previously discussed weakening in geomagnetic activity and the magnetopause return-  
 396 ing closer to its nominal position. The wave activity in the inner magnetosphere also clearly  
 397 subsided: Some hiss and EMIC waves occurred, but the activity was shorter in duration and  
 398 less intense than during the preceding sheath. The Pc5 power, although it remained elevated,  
 399 declined from the level observed during sheath SH3.

### 400 3.3 Period 3: Feb 20–22, 2014

401 Finally, the interval Feb 20–22, 2014 covers the fourth ICME. The radiation belt re-  
 402 sponse, chorus and ULF waves are shown again in the same format as in the previous subsec-  
 403 tions in Figures 9, 10, and 11.

412 Shock S4 was the strongest shock; its magnetosonic Mach number was 6.8 and the  
 413 solar wind speed jumped by almost  $200 \text{ km s}^{-1}$ . We note that as this shock was running into  
 414 the end of ejecta E3, it was preceded by low densities and magnetic fields (about only few  
 415  $\text{cm}^{-3}$  and nT, respectively), and had thus low Alfvén and magnetosonic speeds.

416 Sheath SH4, however, had relatively low dynamic pressure. The steadily declining  
 417 magnetic field magnitude and solar wind speed through this sheath and the following ejecta  
 418 (E4) suggest that this ICME was crossed far from the center (also supported by the per-  
 419 pendicular pressure profile, data not shown, see *Jian et al.* [2006]). Sheath SH4 had large-  
 420 amplitude southward IMF excursions in its leading part that resulted in a new decrease of  
 421 the Dst index and several strong substorms. In the trailing part of the sheath and during the  
 422 ejecta the magnetic field was only weakly southward ( $\sim -5 \text{ nT}$  in GSM). The ring current  
 423 weakened, but some substorms, mostly weak to moderate in magnitude, did occur. The mag-  
 424 netopause was first compressed to a distance of about  $8 R_E$  from the Earth and then moved  
 425 progressively further away from geostationary orbit with the declining dynamic pressure dur-  
 426 ing sheath SH4 and ejecta E4.

427 At the beginning of sheath SH4 the seed population and the core population at 4.2 MeV  
 428 slightly depleted. These depletions occurred when several depleting effects were again ob-  
 429 served: The magnetopause was compressed and ring current enhanced, and Figure 11 shows  
 430 that the Pc5 and EMIC powers were high suggesting outward radial transport and pitch-angle  
 431 scattering losses.

432 After this small depletion, a progressive enhancement of core energies is visible in fig-  
 433 ures 2 and 9, while the variations of the seed population remained relatively modest through-  
 434 out the rest of the studied interval. At 1547-keV energies the flux increase is the strongest  
 435 during the sheath, while at 4.2-MeV energies the most significant enhancement occurred  
 436 later, around the time when the trailing part of ejecta E4 arrives at Earth. The peak of the  
 437 flux moved also to a slightly higher  $L$ -shells, from  $L \simeq 4.5$  to  $L \simeq 5$ . Figure 10 shows rela-  
 438 tively continuous chorus waves (in particular lower band) during both sheath SH4 and ejecta  
 439 E4. As expected, these chorus waves were associated with substorm activity and enhance-  
 440 ments of source electrons. Although the Pc5 power declined from values observed during  
 441 the beginning of sheath SH4, it stayed elevated when compared to quiet time values. We thus  
 442 suggest that these enhancements of core electrons can be related to chorus waves accelerating  
 443 electrons progressively and to radial inward diffusion by ULF waves. We also point out that  
 444 during the trailing part of sheath SH4 and during ejecta E4, the conditions leading to losses  
 445 were mostly absent; the magnetopause was far from the geostationary orbit and the ring cur-  
 446 rent weakened. Strong EMIC power was also mostly absent and hiss was observed only pe-

riodically. A small depletion at core energies during the end part of ejecta E4 coincides with higher EMIC, ULF Pc5, and hiss activity and small decrease in Dst.

#### 4 Discussion and conclusions

In this paper we have analyzed the response of the outer Van Allen radiation belt and wave activity in the inner magnetosphere during a complex solar wind driver event consisting of a series of ICMEs of which the three last ones were closely interacting.

We have collected in Figure 12 an overview of the studied interval. The top three panels show the maximum fluxes of source, seed and core populations as in Figure 2, and the following panels give the time during the 6-hour intervals when chorus, hiss, ULF Pc5, and EMIC powers, subsolar magnetopause position ( $R_{mp}$ ), and Dst and AL indices exceeded certain thresholds (see the figure caption and Table 1). The color-coding of the symbols indicates the large-scale solar wind structure that was influencing the Earth's magnetosphere.

The investigated event featured a strong and sustained (over four days) core electron depletion. The sheath of the first ICME did not cause a magnetic storm, but wiped out most of the pre-existing relativistic electron population. Seed population also depleted significantly and it took several days before the fluxes recovered. A further decrease in fluxes occurred during the southward fields in the second ejecta that deepened for core energies when these fields were compressed by the shock of the third ICME. These results are in agreement with *Hietala et al.* [2014] and *Kilpua et al.* [2015a] who showed that sheaths effectively deplete  $>2$ -MeV electron fluxes at geostationary orbit. We now detail this by demonstrating that depletions occur over wide  $L$ - and energy-ranges and that significant depletions can also occur during the sheaths that do not cause magnetic storms. Our results here are also consistent with *Lugaz et al.* [2015b] who analyzed an event where weakly southward ICME ejecta fields were compressed by a shock, also resulting in a depletion of the outer radiation belt.

Our study also gives evidence for the suggestion by *Hietala et al.* [2014] and *Kilpua et al.* [2015a] that the depleting effect of sheaths is due to combined magnetopause shadowing and precipitation losses. We showed that during the main depletions discussed above, the subsolar magnetopause was strongly compressed or eroded and the wave activity in the inner magnetosphere was diverse and intense (ULF Pc5, EMIC and hiss). In fact, Figure 12 shows that the first and the deepest depletion is associated with the largest percentage of time with strongly compressed  $R_{mp}$  and strong Pc5 and EMIC powers as observed by the GOES 13 and 15 satellites. As discussed in the Introduction, Pc5 fluctuations are expected to enhance magnetopause shadowing losses by the outward radial diffusion, while EMIC and hiss can cause precipitation losses to the atmosphere via pitch-angle scattering. During the first three ejecta in turn the core fluxes experienced very modest variations. This is consistent with *Kilpua et al.* [2015a]. We showed that during these periods the magnetopause stayed closer to its nominal position and strong EMIC power occurred only very sporadically (see also blue dots in Figure 12d). The Pc5 power, although on average enhanced for sustained periods, was generally lower in magnitude than during the sheaths.

The sustained depletion here can thus be attributed to the alternating forcing of the Earth's magnetosphere by sheaths, ejecta and undisturbed slow solar wind that either depleted the belts or caused no significant changes [see also an example of a sheath followed by an ejecta with northward fields in *Alves et al.*, 2016]. *Liu et al.* [2015] studied the period of February 18 – March 2, 2014, including thus also the period studied in this paper. Their general conclusion is that relativistic electrons in the storm main phases at this time decreased due to adiabatic magnetopause shadowing and hiss-induced non-adiabatic processes. As discussed above, we would also stress strong Pc5 ULF wave activity causing outward radial diffusion and scattering by EMIC waves as significant causes of loss, even outside the main phase of a storm.

505 Source electrons were in turn enhanced also during the structures that depleted the  
 506 seed and core populations. In these cases substorms (storm-time or isolated) effectively in-  
 507 jected new electrons in the inner magnetosphere. The strongest source and seed electron en-  
 508 hancements took place during the time when the shock compressed ejecta fields arrived, em-  
 509 phasising the importance of CME interactions in causing considerable changes in the outer  
 510 radiation belt, and during the last ICME for source energies. The substorms and source elec-  
 511 tron enhancements coincided with chorus waves, featured also by similar variations between  
 512 the panels a), f) and, i) in Figure 12. The studied event also highlights that in interacting  
 513 ICMEs solar wind conditions may change relatively quickly, leading to sporadic chorus ac-  
 514 tivity that do not allow acceleration to relativistic energies. In addition, as discussed above,  
 515 conditions that favor the losses of relativistic electrons prevail in such structures.

516 The clearest enhancements of the core electron population in the investigated event  
 517 was caused by the fourth ICME, primarily through its sheath, that made only a glancing en-  
 518 counter with the Earth. Both the sheath and the ejecta of this ICME had low dynamic pres-  
 519 sure and the trailing part of the sheath and the ejecta had only weakly southward magnetic  
 520 fields. These led to the conditions in the inner magnetosphere where effective acceleration  
 521 could take place, but no significant losses occurred. Figure 12 shows that during this period  
 522 strong EMIC and hiss power was sporadic, the ring current weakened and the magnetopause  
 523 was far from geostationary orbit. Strong chorus activity in turn occurred frequently (panel f).  
 524 We suggest that the acceleration to relativistic energies was a combination from local accel-  
 525 eration by chorus waves and inward radial diffusion by Pc5 waves [e.g., *Ma et al.*, 2018]. Our  
 526 results are thus consistent with *Jaynes et al.* [2015] emphasising that sustained chorus waves  
 527 are needed to act for a sufficiently long time to progressively accelerate electrons to MeV en-  
 528 ergies. Another key enhancement at core energies occurred during the beginning of the first  
 529 sheath with predominantly northward IMF and high dynamic pressure. The compression  
 530 during the sheath was related to a significant strengthening of the inner magnetosphere mag-  
 531 netic field. This enhancement caused a gain in electron energy as their drift shells contracted  
 532 and launched ULF Pc5 waves that led to inward radial diffusion [see also *Su et al.*, 2015].

533 To conclude, our study highlights that interacting ICMEs are particularly challeng-  
 534 ing for understanding and forecasting radiation belt dynamics when the Earth's magnetic  
 535 environment is forced alternately by shocks, sheaths, compressed ejecta plasma and mag-  
 536 netic field and ejecta with different magnetic field configurations. The combination of struc-  
 537 tures may vary significantly from event to event. According to this study, while the source  
 538 and seed populations are periodically enhanced, during most of these sub-structures deplet-  
 539 ing effects, both related to magnetopause shadowing and precipitation losses, dominate the  
 540 core electron dynamics, even in the absence of storm main phase, or the chorus wave activ-  
 541 ity is not extended enough to accelerate electrons to relativistic energies. In our study, the  
 542 structures that resulted in significant core energy enhancements were an ICME encountered  
 543 through its flank and a sheath with northward magnetic field and strong dynamic pressure.  
 544 The former caused continuous chorus and Pc5 wave activity and the latter positive Dst effect  
 545 and ULF wave-induced radial diffusion. Both structures also largely lacked depleting effects.  
 546 Detailed knowledge of typical acceleration, transport and loss processes in different substruc-  
 547 tures allow understanding also the response to the complex drivers.

## 548 Acknowledgments

549 The authors are thankful to all of the Van Allen Probes, Wind, and OMNI teams for making  
 550 their data available to the public. The OMNI and Wind data were obtained through CDAWeb  
 551 (<https://cdaweb.sci.gsfc.nasa.gov/index.html/>). We thank Craig Kletzing and  
 552 the EMFISIS team for Van Allen Probes density data ([https://emfisis.160physics.  
 553 uiowa.edu/data/index](https://emfisis.160physics.uiowa.edu/data/index)), and Harlan Spence and the ECT team for Van Allen Probes  
 554 MagEIS and REPT electron flux data ([https://rbsp-ect.lanl.gov/science/DataDirectories.  
 555 php](https://rbsp-ect.lanl.gov/science/DataDirectories.php)). EK acknowledges the European Research Council (ERC) under the European Union's  
 556 Horizon 2020 Research and Innovation Programme Project SolMAG 724391, and Academy

557 of Finland Project 1310445. The results presented in here have been achieved under the  
 558 framework of the Finnish Centre of Excellence in Research of Sustainable Space (Academy  
 559 of Finland grant number 1312390), which we gratefully acknowledge. HH is supported by  
 560 the Turku Collegium of Science and Medicine. Work at The Aerospace Corporation was  
 561 supported by RBSP-ECT funding provided by JHU/APL contract 967399 under NASA's  
 562 prime contract NAS5-01072

## 563 References

- 564 Alves, L. R., L. A. Da Silva, V. M. Souza, D. G. Sibeck, P. R. Jauer, L. E. A. Vieira, B. M.  
 565 Walsh, M. V. D. Silveira, J. P. Marchezi, M. Rockenbach, A. D. Lago, O. Mendes, B. T.  
 566 Tsurutani, D. Koga, S. G. Kanekal, D. N. Baker, J. R. Wygant, and C. A. Kletzing (2016),  
 567 Outer radiation belt dropout dynamics following the arrival of two interplanetary coronal  
 568 mass ejections, *Geophys. Res. Lett.*, *43*, 978–987, doi:10.1002/2015GL067066.
- 569 Artemyev, A., O. Agapitov, D. Mourenas, V. Krasnoselskikh, V. Shastun, and F. Mozer  
 570 (2016), Oblique Whistler-Mode Waves in the Earth's Inner Magnetosphere: Energy Dis-  
 571 tribution, Origins, and Role in Radiation Belt Dynamics, *Space Sci. Rev.*, *200*, 261–355,  
 572 doi:10.1007/s11214-016-0252-5.
- 573 Artemyev, A. V., A. A. Vasiliev, D. Mourenas, O. V. Agapitov, V. Krasnoselskikh,  
 574 D. Boscher, and G. Rolland (2014), Fast transport of resonant electrons in phase space  
 575 due to nonlinear trapping by whistler waves, *Geophys. Res. Lett.*, *41*, 5727–5733, doi:  
 576 10.1002/2014GL061380.
- 577 Aubry, M. P., C. T. Russell, and M. G. Kivelson (1970), Inward motion of the magnetopause  
 578 before a substorm, *J. Geophys. Res.*, *75*, 7018, doi:10.1029/JA075i034p07018.
- 579 Baker, D. N., S. G. Kanekal, V. C. Hoxie, M. G. Henderson, X. Li, H. E. Spence, S. R.  
 580 Elkington, R. H. W. Friedel, J. Goldstein, M. K. Hudson, G. D. Reeves, R. M. Thorne,  
 581 C. A. Kletzing, and S. G. Claudepierre (2013a), A Long-Lived Relativistic Electron  
 582 Storage Ring Embedded in Earth's Outer Van Allen Belt, *Science*, *340*, 186–190, doi:  
 583 10.1126/science.1233518.
- 584 Baker, D. N., S. G. Kanekal, V. C. Hoxie, S. Batiste, M. Bolton, X. Li, S. R. Elkington,  
 585 S. Monk, R. Reukauf, S. Steg, J. Westfall, C. Belting, B. Bolton, D. Braun, B. Cervelli,  
 586 K. Hubbell, M. Kien, S. Knappmiller, S. Wade, B. Lamprecht, K. Stevens, J. Wallace,  
 587 A. Yehle, H. E. Spence, and R. Friedel (2013b), The Relativistic Electron-Proton Tele-  
 588 scope (REPT) Instrument on Board the Radiation Belt Storm Probes (RBSP) Spacecraft:  
 589 Characterization of Earth's Radiation Belt High-Energy Particle Populations, *Space Sci.*  
 590 *Rev.*, *179*, 337–381, doi:10.1007/s11214-012-9950-9.
- 591 Baker, D. N., A. N. Jaynes, X. Li, M. G. Henderson, S. G. Kanekal, G. D. Reeves, H. E.  
 592 Spence, S. G. Claudepierre, J. F. Fennell, M. K. Hudson, R. M. Thorne, J. C. Foster, P. J.  
 593 Erickson, D. M. Malaspina, J. R. Wygant, A. Boyd, C. A. Kletzing, A. Drozdov, and Y. Y.  
 594 Shprits (2014), Gradual diffusion and punctuated phase space density enhancements of  
 595 highly relativistic electrons: Van Allen Probes observations, *Geophys. Res. Lett.*, *41*,  
 596 1351–1358, doi:10.1002/2013GL058942.
- 597 Baker, D. N., P. J. Erickson, J. F. Fennell, J. C. Foster, A. N. Jaynes, and P. T. Verronen  
 598 (2018), Space Weather Effects in the Earth's Radiation Belts, *Space Sci. Rev.*, *214*, 17,  
 599 doi:10.1007/s11214-017-0452-7.
- 600 Blake, J. B., P. A. Carranza, S. G. Claudepierre, J. H. Clemmons, W. R. Crain, Y. Dotan,  
 601 J. F. Fennell, F. H. Fuentes, R. M. Galvan, J. S. George, M. G. Henderson, M. Lalic, A. Y.  
 602 Lin, M. D. Looper, D. J. Mabry, J. E. Mazur, B. McCarthy, C. Q. Nguyen, T. P. O'Brien,  
 603 M. A. Perez, M. T. Redding, J. L. Roeder, D. J. Salvaggio, G. A. Sorensen, H. E. Spence,  
 604 S. Yi, and M. P. Zakrzewski (2013), The Magnetic Electron Ion Spectrometer (MagEIS)  
 605 Instruments Aboard the Radiation Belt Storm Probes (RBSP) Spacecraft, *Space Sci. Rev.*,  
 606 *179*, 383–421, doi:10.1007/s11214-013-9991-8.
- 607 Bortnik, J., R. M. Thorne, and N. P. Meredith (2008), The unexpected origin of plasmas-  
 608 pheric hiss from discrete chorus emissions, *Nature*, *452*, 62–66, doi:10.1038/nature06741.

- 609 Boyd, A. J., D. L. Turner, G. D. Reeves, H. E. Spence, D. N. Baker, and J. B. Blake (2018),  
 610 What Causes Radiation Belt Enhancements: A Survey of the Van Allen Probes Era, *Geo-*  
 611 *phys. Res. Lett.*, *45*, 5253–5259, doi:10.1029/2018GL077699.
- 612 Brito, T., L. Woodger, M. Hudson, and R. Millan (2012), Energetic radiation belt electron  
 613 precipitation showing ULF modulation, *Geophys. Res. Lett.*, *39*, L22104, doi:10.1029/  
 614 2012GL053790.
- 615 Califf, S., X. Li, H. Zhao, A. Kellerman, T. E. Sarris, A. Jaynes, and D. M. Malaspina  
 616 (2017), The role of the convection electric field in filling the slot region between the inner  
 617 and outer radiation belts, *Journal of Geophysical Research (Space Physics)*, *122*, 2051–  
 618 2068, doi:10.1002/2016JA023657.
- 619 Cattell, C. A., A. W. Breneman, S. A. Thaller, J. R. Wygant, C. A. Kletzing, and W. S. Kurth  
 620 (2015), Van Allen Probes observations of unusually low frequency whistler mode waves  
 621 observed in association with moderate magnetic storms: Statistical study, *Geophys. Res.*  
 622 *Lett.*, *42*, 7273–7281, doi:10.1002/2015GL065565.
- 623 Claudepierre, S. G., S. R. Elkington, and M. Wiltberger (2008), Solar wind driving of mag-  
 624 netospheric ULF waves: Pulsations driven by velocity shear at the magnetopause, *Journal*  
 625 *of Geophysical Research (Space Physics)*, *113*, A05218, doi:10.1029/2007JA012890.
- 626 Claudepierre, S. G., M. K. Hudson, W. Lotko, J. G. Lyon, and R. E. Denton (2010), Solar  
 627 wind driving of magnetospheric ULF waves: Field line resonances driven by dynamic  
 628 pressure fluctuations, *Journal of Geophysical Research (Space Physics)*, *115*, A11202,  
 629 doi:10.1029/2010JA015399.
- 630 Douma, E., C. J. Rodger, L. W. Blum, and M. A. Clilverd (2017), Occurrence characteristics  
 631 of relativistic electron microbursts from SAMPEX observations, *Journal of Geophysical*  
 632 *Research (Space Physics)*, *122*, 8096–8107, doi:10.1002/2017JA024067.
- 633 Elkington, S. R., M. K. Hudson, and A. A. Chan (2003), Resonant acceleration and diffu-  
 634 sion of outer zone electrons in an asymmetric geomagnetic field, *Journal of Geophysical*  
 635 *Research (Space Physics)*, *108*, 1116, doi:10.1029/2001JA009202.
- 636 Engebretson, M. J., J. L. Posch, D. J. Braun, W. Li, Q. Ma, A. C. Kellerman, C.-L. Huang,  
 637 S. G. Kanekal, C. A. Kletzing, J. R. Wygant, H. E. Spence, D. N. Baker, J. F. Fennell,  
 638 V. Angelopoulos, H. J. Singer, M. R. Lessard, R. B. Horne, T. Raita, K. Shiokawa,  
 639 R. Rakhmatulin, E. Dmitriev, and E. Ermakova (2018), Emic wave events during the four  
 640 gem qarb challenge intervals, *Journal of Geophysical Research: Space Physics*, *123*(8),  
 641 6394–6423, doi:10.1029/2018JA025505.
- 642 Foster, J. C., P. J. Erickson, D. N. Baker, S. G. Claudepierre, C. A. Kletzing, W. Kurth, G. D.  
 643 Reeves, S. A. Thaller, H. E. Spence, Y. Y. Shprits, and J. R. Wygant (2014), Prompt en-  
 644 ergization of relativistic and highly relativistic electrons during a substorm interval: Van  
 645 Allen Probes observations, *Geophys. Res. Lett.*, *41*, 20–25, doi:10.1002/2013GL058438.
- 646 Foster, J. C., J. R. Wygant, M. K. Hudson, A. J. Boyd, D. N. Baker, P. J. Erickson, and H. E.  
 647 Spence (2015), Shock-induced prompt relativistic electron acceleration in the inner mag-  
 648 netosphere, *Journal of Geophysical Research (Space Physics)*, *120*, 1661–1674, doi:  
 649 10.1002/2014JA020642.
- 650 Green, J. C., J. Likar, and Y. Shprits (2017), Impact of space weather on the satellite indus-  
 651 try, *Space Weather*, *15*, 804–818, doi:10.1002/2017SW001646.
- 652 Hartinger, M. D., D. L. Turner, F. Plaschke, V. Angelopoulos, and H. Singer (2013), The  
 653 role of transient ion foreshock phenomena in driving Pc5 ULF wave activity, *Journal of*  
 654 *Geophysical Research (Space Physics)*, *118*, 299–312, doi:10.1029/2012JA018349.
- 655 Hartley, D. P., C. A. Kletzing, O. Santolík, L. Chen, and R. B. Horne (2018), Statistical  
 656 Properties of Plasmaspheric Hiss From Van Allen Probes Observations, *Journal of Geo-*  
 657 *physical Research (Space Physics)*, *123*, 2605–2619, doi:10.1002/2017JA024593.
- 658 Hietala, H., E. K. J. Kilpua, D. L. Turner, and V. Angelopoulos (2014), Depleting effects of  
 659 ICME-driven sheath regions on the outer electron radiation belt, *Geophys. Res. Lett.*, *41*,  
 660 2258–2265, doi:10.1002/2014GL059551.
- 661 Horne, R. B., and R. M. Thorne (1998), Potential waves for relativistic electron scattering  
 662 and stochastic acceleration during magnetic storms, *Geophys. Res. Lett.*, *25*, 3011–3014,

- doi:10.1029/98GL01002.
- 663  
664 Hudson, M. K., B. T. Kress, H.-R. Mueller, J. A. Zastrow, and J. Bernard Blake (2008), Rela-  
665 tionship of the Van Allen radiation belts to solar wind drivers, *Journal of Atmospheric and*  
666 *Solar-Terrestrial Physics*, *70*, 708–729, doi:10.1016/j.jastp.2007.11.003.
- 667 Jaynes, A. N., D. N. Baker, H. J. Singer, J. V. Rodriguez, T. M. Loto'aniu, A. F. Ali, S. R.  
668 Elkington, X. Li, S. G. Kanekal, J. F. Fennell, W. Li, R. M. Thorne, C. A. Kletzing, H. E.  
669 Spence, and G. D. Reeves (2015), Source and seed populations for relativistic electrons:  
670 Their roles in radiation belt changes, *Journal of Geophysical Research (Space Physics)*,  
671 *120*, 7240–7254, doi:10.1002/2015JA021234.
- 672 Jian, L., C. T. Russell, J. G. Luhmann, and R. M. Skoug (2006), Properties of Interplanetary  
673 Coronal Mass Ejections at One AU During 1995–2004, *Sol. Phys.*, *239*, 393–436, doi:10.  
674 1007/s11207-006-0133-2.
- 675 Kanekal, S. G., D. N. Baker, J. F. Fennell, A. Jones, Q. Schiller, I. G. Richardson, X. Li,  
676 D. L. Turner, S. Califf, S. G. Claudepierre, L. B. Wilson, III, A. Jaynes, J. B. Blake, G. D.  
677 Reeves, H. E. Spence, C. A. Kletzing, and J. R. Wygant (2016), Prompt acceleration of  
678 magnetospheric electrons to ultrarelativistic energies by the 17 March 2015 interplan-  
679 etary shock, *Journal of Geophysical Research (Space Physics)*, *121*, 7622–7635, doi:  
680 10.1002/2016JA022596.
- 681 Kepko, L., and H. E. Spence (2003), Observations of discrete, global magnetospheric oscil-  
682 lations directly driven by solar wind density variations, *Journal of Geophysical Research*  
683 *(Space Physics)*, *108*, 1257, doi:10.1029/2002JA009676.
- 684 Kersten, T., R. B. Horne, S. A. Glauert, N. P. Meredith, B. J. Fraser, and R. S. Grew (2014),  
685 Electron losses from the radiation belts caused by EMIC waves, *Journal of Geophysical*  
686 *Research (Space Physics)*, *119*, 8820–8837, doi:10.1002/2014JA020366.
- 687 Kessel, M. (2016), Things we do not yet understand about solar driving of the radiation  
688 belts, *Journal of Geophysical Research (Space Physics)*, *121*, 5549–5552, doi:10.1002/  
689 2016JA022472.
- 690 Kilpua, E., H. E. J. Koskinen, and T. I. Pulkkinen (2017a), Coronal mass ejections and  
691 their sheath regions in interplanetary space, *Living Reviews in Solar Physics*, *14*, 5, doi:  
692 10.1007/s41116-017-0009-6.
- 693 Kilpua, E. K. J., H. Hietala, D. L. Turner, H. E. J. Koskinen, T. I. Pulkkinen, J. V. Rodriguez,  
694 G. D. Reeves, S. G. Claudepierre, and H. E. Spence (2015a), Unraveling the drivers of  
695 the storm time radiation belt response, *Geophys. Res. Lett.*, *42*, 3076–3084, doi:10.1002/  
696 2015GL063542.
- 697 Kilpua, E. K. J., E. Lumme, K. Andreeova, A. Isavnin, and H. E. J. Koskinen (2015b),  
698 Properties and drivers of fast interplanetary shocks near the orbit of the Earth (1995-  
699 2013), *Journal of Geophysical Research (Space Physics)*, *120*, 4112–4125, doi:10.1002/  
700 2015JA021138.
- 701 Kilpua, E. K. J., A. Balogh, R. von Steiger, and Y. D. Liu (2017b), Geoeffective Properties  
702 of Solar Transients and Stream Interaction Regions, *Space Sci. Rev.*, *212*, 1271–1314, doi:  
703 10.1007/s11214-017-0411-3.
- 704 Kim, H.-J., and A. A. Chan (1997), Fully adiabatic changes in storm time relativistic electron  
705 fluxes, *J. Geophys. Res.*, *102*, 22,107–22,116, doi:10.1029/97JA01814.
- 706 Kletzing, C. A., W. S. Kurth, M. Acuna, R. J. MacDowall, R. B. Torbert, T. Averkamp,  
707 D. Bodet, S. R. Bounds, M. Chutter, J. Connerney, D. Crawford, J. S. Dolan, R. Dvorsky,  
708 G. B. Hospodarsky, J. Howard, V. Jordanova, R. A. Johnson, D. L. Kirchner, B. Mokrzy-  
709 cki, G. Needell, J. Odom, D. Mark, R. Pfaff, J. R. Phillips, C. W. Piker, S. L. Reming-  
710 ton, D. Rowland, O. Santolik, R. Schnurr, D. Sheppard, C. W. Smith, R. M. Thorne, and  
711 J. Tyler (2013), The Electric and Magnetic Field Instrument Suite and Integrated Science  
712 (EMFISIS) on RBSP, *Space Sci. Rev.*, *179*, 127–181, doi:10.1007/s11214-013-9993-6.
- 713 Lam, M. M., R. B. Horne, N. P. Meredith, S. A. Glauert, T. Moffat-Griffin, and J. C. Green  
714 (2010), Origin of energetic electron precipitation >30 keV into the atmosphere, *Journal of*  
715 *Geophysical Research (Space Physics)*, *115*, A00F08, doi:10.1029/2009JA014619.

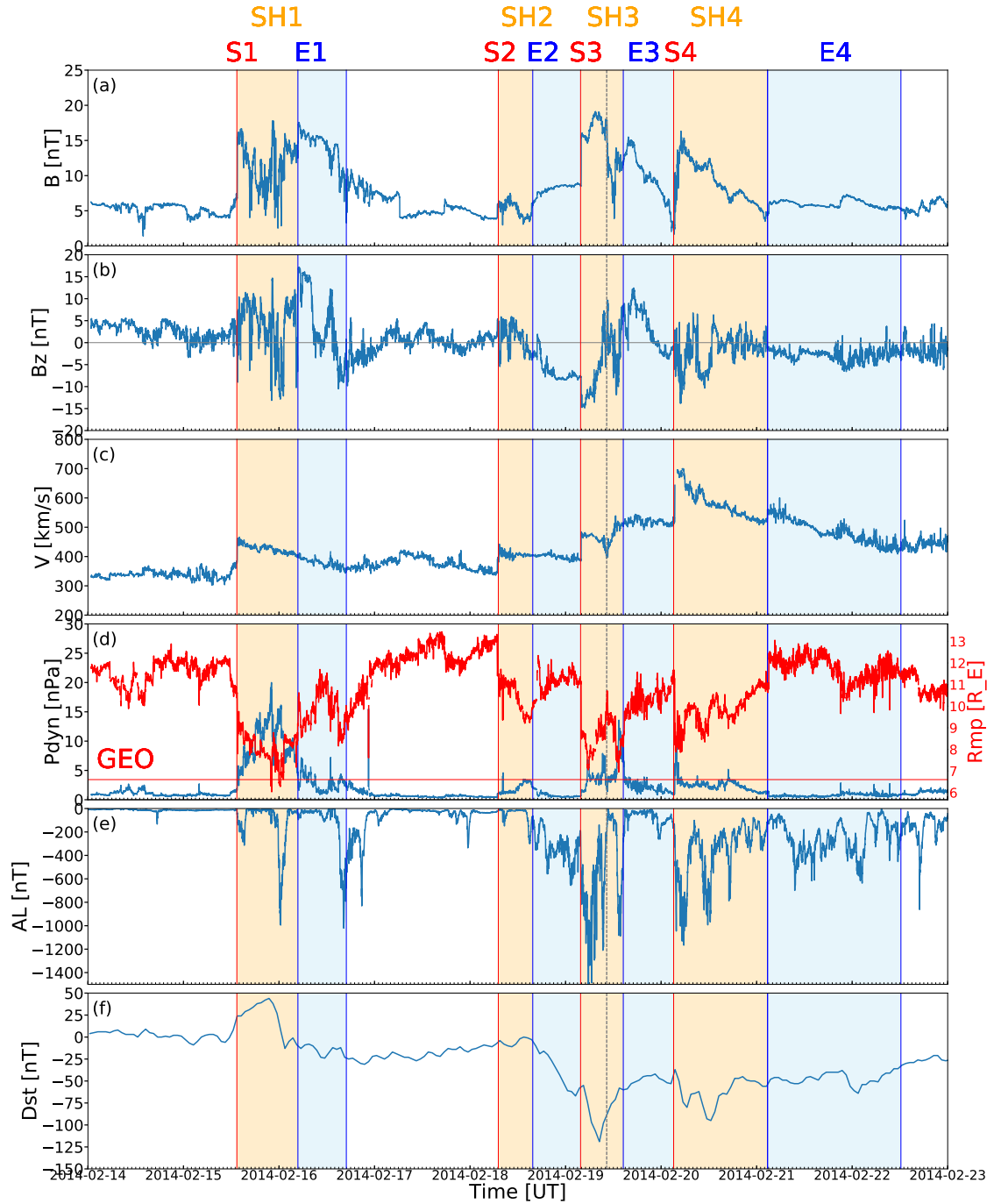
- 716 Li, W., R. M. Thorne, Q. Ma, B. Ni, J. Bortnik, D. N. Baker, H. E. Spence, G. D. Reeves,  
717 S. G. Kanekal, J. C. Green, C. A. Kletzing, W. S. Kurth, G. B. Hospodarsky, J. B. Blake,  
718 J. F. Fennell, and S. G. Claudepierre (2014), Radiation belt electron acceleration by chorus  
719 waves during the 17 March 2013 storm, *Journal of Geophysical Research (Space Physics)*,  
720 *119*, 4681–4693, doi:10.1002/2014JA019945.
- 721 Li, X., D. N. Baker, M. Temerin, T. E. Cayton, E. G. D. Reeves, R. A. Christensen, J. B.  
722 Blake, M. D. Looper, R. Nakamura, and S. G. Kanekal (1997), Multisatellite observations  
723 of the outer zone electron variation during the November 3–4, 1993, magnetic storm, *J.*  
724 *Geophys. Res.*, *102*, 14,123–14,140, doi:10.1029/97JA01101.
- 725 Liu, S., F. Xiao, C. Yang, Y. He, Q. Zhou, C. A. Kletzing, W. S. Kurth, G. B. Hospodarsky,  
726 H. E. Spence, G. D. Reeves, H. O. Funsten, J. B. Blake, D. N. Baker, and J. R. Wygant  
727 (2015), Van Allen Probes observations linking radiation belt electrons to chorus waves  
728 during 2014 multiple storms, *Journal of Geophysical Research (Space Physics)*, *120*, 938–  
729 948, doi:10.1002/2014JA020781.
- 730 Lugaz, N., C. J. Farrugia, C. W. Smith, and K. Paulson (2015a), Shocks inside CMEs: A  
731 survey of properties from 1997 to 2006, *Journal of Geophysical Research (Space Physics)*,  
732 *120*, 2409–2427, doi:10.1002/2014JA020848.
- 733 Lugaz, N., C. J. Farrugia, C. W. Smith, and K. Paulson (2015b), Shocks inside CMEs: A  
734 survey of properties from 1997 to 2006, *Journal of Geophysical Research (Space Physics)*,  
735 *120*, 2409–2427, doi:10.1002/2014JA020848.
- 736 Lugaz, N., C. J. Farrugia, R. M. Winslow, N. Al-Haddad, E. K. J. Kilpua, and P. Riley  
737 (2016), Factors affecting the geoeffectiveness of shocks and sheaths at 1 AU, *Journal of*  
738 *Geophysical Research (Space Physics)*, *121*, 10, doi:10.1002/2016JA023100.
- 739 Ma, Q., W. Li, J. Bortnik, R. M. Thorne, X. Chu, L. G. Ozeke, G. D. Reeves, C. A. Kletz-  
740 ing, W. S. Kurth, G. B. Hospodarsky, M. J. Engebretson, H. E. Spence, D. N. Baker, J. B.  
741 Blake, J. F. Fennell, and S. G. Claudepierre (2018), Quantitative Evaluation of Radial Dif-  
742 fusion and Local Acceleration Processes During GEM Challenge Events, *Journal of Geo-*  
743 *physical Research (Space Physics)*, *123*, 1938–1952, doi:10.1002/2017JA025114.
- 744 Mann, I. R., L. G. Ozeke, K. R. Murphy, S. G. Claudepierre, D. L. Turner, D. N. Baker,  
745 I. J. Rae, A. Kale, D. K. Milling, A. J. Boyd, H. E. Spence, G. D. Reeves, H. J. Singer,  
746 S. Dimitrakoudis, I. A. Daglis, and F. Honary (2016), Explaining the dynamics of  
747 the ultra-relativistic third Van Allen radiation belt, *Nature Physics*, *12*, 978–983, doi:  
748 10.1038/nphys3799.
- 749 Mauk, B. H., N. J. Fox, S. G. Kanekal, R. L. Kessel, D. G. Sibeck, and A. Ukhorskiy (2013),  
750 Science Objectives and Rationale for the Radiation Belt Storm Probes Mission, *Space Sci.*  
751 *Rev.*, *179*, 3–27, doi:10.1007/s11214-012-9908-y.
- 752 Mayaud, P. (1980), *Derivation, Meaning, and Use of Geomagnetic Indices*, *Geophysical*  
753 *Monograph*, vol. 22, American Geophysical Union, Washington, DC.
- 754 Meredith, N. P., R. B. Horne, R. H. A. Iles, R. M. Thorne, D. Heynderickx, and R. R. An-  
755 derson (2002), Outer zone relativistic electron acceleration associated with substorm-  
756 enhanced whistler mode chorus, *Journal of Geophysical Research (Space Physics)*, *107*,  
757 1144, doi:10.1029/2001JA900146.
- 758 Meredith, N. P., R. M. Thorne, R. B. Horne, D. Summers, B. J. Fraser, and R. R. Anderson  
759 (2003), Statistical analysis of relativistic electron energies for cyclotron resonance with  
760 EMIC waves observed on CRRES, *Journal of Geophysical Research (Space Physics)*, *108*,  
761 1250, doi:10.1029/2002JA009700.
- 762 Meredith, N. P., R. B. Horne, S. A. Glauert, R. M. Thorne, D. Summers, J. M. Albert, and  
763 R. R. Anderson (2006), Energetic outer zone electron loss timescales during low geo-  
764 magnetic activity, *Journal of Geophysical Research (Space Physics)*, *111*, A05212, doi:  
765 10.1029/2005JA011516.
- 766 Miyoshi, Y., R. Kataoka, Y. Kasahara, A. Kumamoto, T. Nagai, and M. F. Thomsen (2013),  
767 High-speed solar wind with southward interplanetary magnetic field causes relativistic  
768 electron flux enhancement of the outer radiation belt via enhanced condition of whistler  
769 waves, *Geophys. Res. Lett.*, *40*, 4520–4525, doi:10.1002/grl.50916.

- 770 Nieves-Chinchilla, T., A. Vourlidas, J. C. Raymond, M. G. Linton, N. Al-haddad, N. P. Sa-  
 771 vani, A. Szabo, and M. A. Hidalgo (2018), Understanding the Internal Magnetic Field  
 772 Configurations of ICMEs Using More than 20 Years of Wind Observations, , 293, 25, doi:  
 773 10.1007/s11207-018-1247-z.
- 774 O'Brien, T. P. (2009), SEAES-GEO: A spacecraft environmental anomalies expert system  
 775 for geosynchronous orbit, *Space Weather*, 7, 09003, doi:10.1029/2009SW000473.
- 776 Olson, W. P., and K. A. Pfizter (1977), Magnetospheric magnetic field modeling, *Tech. rep.*
- 777 Osmane, A., L. B. Wilson, III, L. Blum, and T. I. Pulkkinen (2016), On the Connection be-  
 778 tween Microbursts and Nonlinear Electronic Structures in Planetary Radiation Belts, , 816,  
 779 51, doi:10.3847/0004-637X/816/2/51.
- 780 Rae, I. J., E. F. Donovan, I. R. Mann, F. R. Fenrich, C. E. J. Watt, D. K. Milling, M. Lester,  
 781 B. Lavraud, J. A. Wild, H. J. Singer, H. Rème, and A. Balogh (2005), Evolution and char-  
 782 acteristics of global Pc5 ULF waves during a high solar wind speed interval, *Journal of*  
 783 *Geophysical Research (Space Physics)*, 110, A12211, doi:10.1029/2005JA011007.
- 784 Reeves, G. D., K. L. McAdams, R. H. W. Friedel, and T. P. O'Brien (2003), Acceleration and  
 785 loss of relativistic electrons during geomagnetic storms, *Geophys. Res. Lett.*, 30, 1529,  
 786 doi:10.1029/2002GL016513.
- 787 Reeves, G. D., H. E. Spence, M. G. Henderson, S. K. Morley, R. H. W. Friedel, H. O. Fun-  
 788 sten, D. N. Baker, S. G. Kanekal, J. B. Blake, J. F. Fennell, S. G. Claudepierre, R. M.  
 789 Thorne, D. L. Turner, C. A. Kletzing, W. S. Kurth, B. A. Larsen, and J. T. Niehof (2013),  
 790 Electron Acceleration in the Heart of the Van Allen Radiation Belts, *Science*, 341, 991–  
 791 994, doi:10.1126/science.1237743.
- 792 Reeves, G. D., R. H. W. Friedel, B. A. Larsen, R. M. Skoug, H. O. Funsten, S. G. Claude-  
 793 pierre, J. F. Fennell, D. L. Turner, M. H. Denton, H. E. Spence, J. B. Blake, and D. N.  
 794 Baker (2016), Energy-dependent dynamics of keV to MeV electrons in the inner zone,  
 795 outer zone, and slot regions, *Journal of Geophysical Research (Space Physics)*, 121, 397–  
 796 412, doi:10.1002/2015JA021569.
- 797 Richardson, I. G. (2018), Solar wind stream interaction regions throughout the heliosphere,  
 798 *Living Reviews in Solar Physics*, 15, 1, doi:10.1007/s41116-017-0011-z.
- 799 Selesnick, R. S., J. B. Blake, and R. A. Mewaldt (2003), Atmospheric losses of radiation  
 800 belt electrons, *Journal of Geophysical Research (Space Physics)*, 108, 1468, doi:10.1029/  
 801 2003JA010160.
- 802 Shprits, Y. Y., S. R. Elkington, N. P. Meredith, and D. A. Subbotin (2008), Review of mod-  
 803 eling of losses and sources of relativistic electrons in the outer radiation belt I: Radial  
 804 transport, *Journal of Atmospheric and Solar-Terrestrial Physics*, 70, 1679–1693, doi:  
 805 10.1016/j.jastp.2008.06.008.
- 806 Shue, J.-H., P. Song, C. T. Russell, J. T. Steinberg, J. K. Chao, G. Zastenker, O. L. Vaisberg,  
 807 S. Kokubun, H. J. Singer, T. R. Detman, and H. Kawano (1998), Magnetopause location  
 808 under extreme solar wind conditions, *J. Geophys. Res.*, 103, 17,691–17,700, doi:10.1029/  
 809 98JA01103.
- 810 Singer, H., L. Matheson, R. Grubb, A. Newman, and D. Bouwer (1996), Monitoring space  
 811 weather with the GOES magnetometers, in *GOES-8 and Beyond, Proceedings of the SPIE*,  
 812 vol. 2812, edited by E. R. Washwell, pp. 299–308, doi:10.1117/12.254077.
- 813 Smith, A. J., M. P. Freeman, and G. D. Reeves (1996), Postmidnight VLF chorus events,  
 814 a substorm signature observed at the ground near L=4, *J. Geophys. Res.*, 101, 24,641–  
 815 24,654, doi:10.1029/96JA02236.
- 816 Su, Z., H. Zhu, F. Xiao, Q.-G. Zong, X.-Z. Zhou, H. Zheng, Y. Wang, S. Wang, Y.-X. Hao,  
 817 Z. Gao, Z. He, D. N. Baker, H. E. Spence, G. D. Reeves, J. B. Blake, and J. R. Wygant  
 818 (2015), Ultra-low-frequency wave-driven diffusion of radiation belt relativistic electrons,  
 819 *Nature Communications*, 6, 10096, doi:10.1038/ncomms10096.
- 820 Summers, D., and C.-y. Ma (2000), A model for generating relativistic electrons in the  
 821 Earth's inner magnetosphere based on gyroresonant wave-particle interactions, *J. Geo-  
 822 phys. Res.*, 105, 2625–2640, doi:10.1029/1999JA900444.

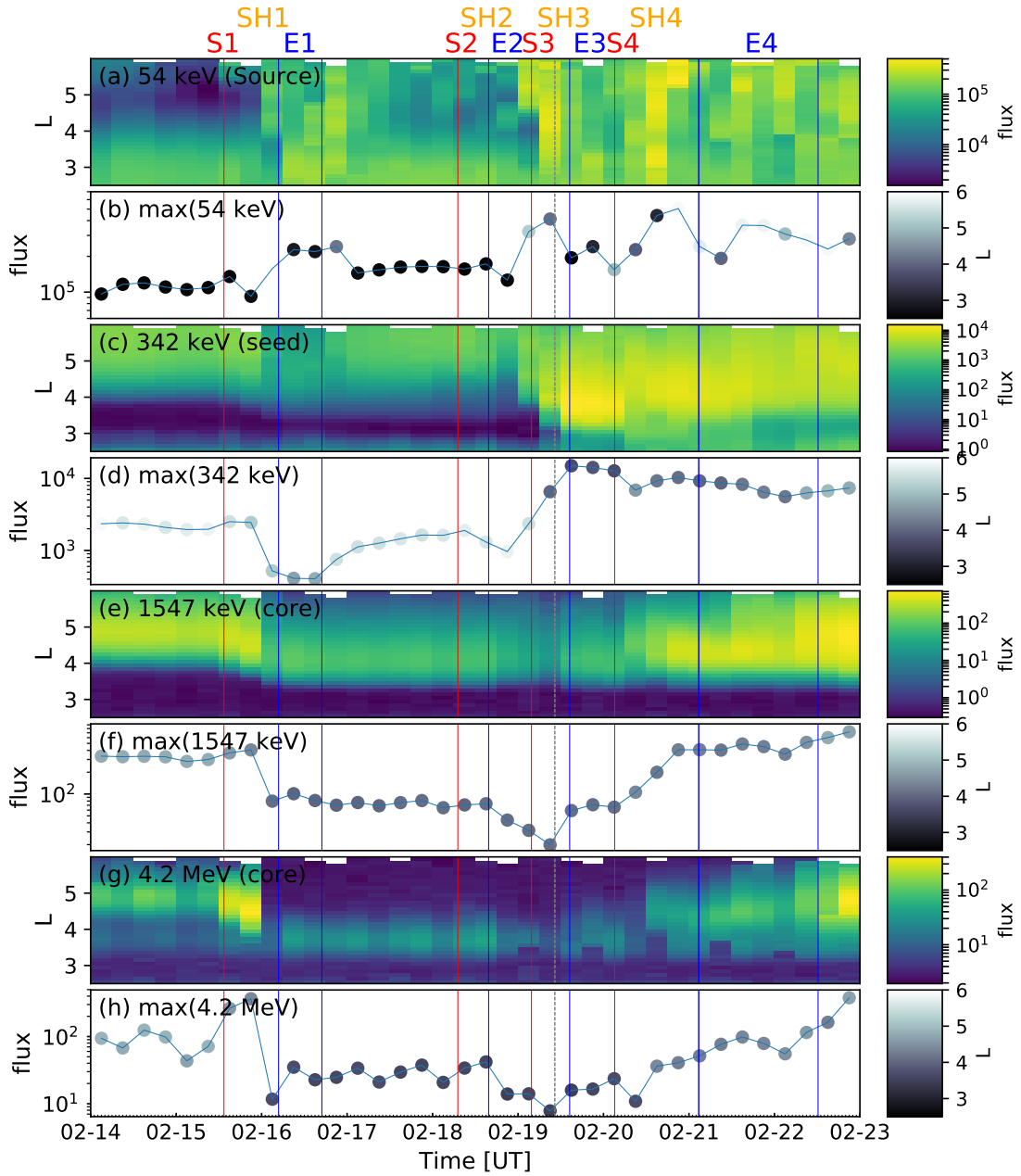


- 823 Summers, D., and R. M. Thorne (2003), Relativistic electron pitch-angle scattering by elec-  
824 tromagnetic ion cyclotron waves during geomagnetic storms, *Journal of Geophysical Re-*  
825 *search (Space Physics)*, *108*, 1143, doi:10.1029/2002JA009489.
- 826 Summers, D., B. Ni, and N. P. Meredith (2007), Timescales for radiation belt electron ac-  
827 celeration and loss due to resonant wave-particle interactions: 2. Evaluation for VLF cho-  
828 rus, ELF hiss, and electromagnetic ion cyclotron waves, *Journal of Geophysical Research*  
829 *(Space Physics)*, *112*, A04207, doi:10.1029/2006JA011993.
- 830 Summers, D., Y. Omura, S. Nakamura, and C. A. Kletzing (2014), Fine structure of plas-  
831 maspheric hiss, *Journal of Geophysical Research (Space Physics)*, *119*, 9134–9149, doi:  
832 10.1002/2014JA020437.
- 833 Thorne, R. M., E. J. Smith, R. K. Burton, and R. E. Holzer (1973), Plasmaspheric hiss, *J.*  
834 *Geophys. Res.*, *78*, 1581–1596, doi:10.1029/JA078i010p01581.
- 835 Thorne, R. M., T. P. O’Brien, Y. Y. Shprits, D. Summers, and R. B. Horne (2005), Timescale  
836 for MeV electron microburst loss during geomagnetic storms, *Journal of Geophysical Re-*  
837 *search (Space Physics)*, *110*, A09202, doi:10.1029/2004JA010882.
- 838 Thorne, R. M., W. Li, B. Ni, Q. Ma, J. Bortnik, L. Chen, D. N. Baker, H. E. Spence, G. D.  
839 Reeves, M. G. Henderson, C. A. Kletzing, W. S. Kurth, G. B. Hospodarsky, J. B. Blake,  
840 J. F. Fennell, S. G. Claudepierre, and S. G. Kanekal (2013), Rapid local acceleration of  
841 relativistic radiation-belt electrons by magnetospheric chorus, *Nature*, *504*, 411–414, doi:  
842 10.1038/nature12889.
- 843 Tsyganenko, N. A., and M. I. Sitnov (2005), Modeling the dynamics of the inner magne-  
844 tosphere during strong geomagnetic storms, *Journal of Geophysical Research (Space*  
845 *Physics)*, *110*, A03208, doi:10.1029/2004JA010798.
- 846 Turner, D. L., V. Angelopoulos, W. Li, M. D. Hartinger, M. Usanova, I. R. Mann, J. Bortnik,  
847 and Y. Shprits (2013), On the storm-time evolution of relativistic electron phase space  
848 density in Earth’s outer radiation belt, *Journal of Geophysical Research (Space Physics)*,  
849 *118*, 2196–2212, doi:10.1002/jgra.50151.
- 850 Turner, D. L., V. Angelopoulos, W. Li, J. Bortnik, B. Ni, Q. Ma, R. M. Thorne, S. K. Morley,  
851 M. G. Henderson, G. D. Reeves, M. Usanova, I. R. Mann, S. G. Claudepierre, J. B. Blake,  
852 D. N. Baker, C.-L. Huang, H. Spence, W. Kurth, C. Kletzing, and J. V. Rodriguez (2014),  
853 Competing source and loss mechanisms due to wave-particle interactions in Earth’s outer  
854 radiation belt during the 30 September to 3 October 2012 geomagnetic storm, *Journal of*  
855 *Geophysical Research (Space Physics)*, *119*, 1960–1979, doi:10.1002/2014JA019770.
- 856 Turner, D. L., T. P. O’Brien, J. F. Fennell, S. G. Claudepierre, J. B. Blake, E. K. J. Kilpua,  
857 and H. Hietala (2015), The effects of geomagnetic storms on electrons in Earth’s radiation  
858 belts, *Geophys. Res. Lett.*, *42*, 9176–9184, doi:10.1002/2015GL064747.
- 859 Turner, D. L., E. K. J. Kilpua, Hietala, S. G. Claudepierre, T. P. O’Brien, J. F. Fennell, J. B.  
860 Blake, A. L. Jaynes, S. Kankal, D. N. Baker, H. E. Spence, J. F. Ripoll, and G. D. Reeves  
861 (2019), The Response of Earth’s Electron Radiation Belts to Geomagnetic Storms: Statis-  
862 tics From the Van Allen Probes Era Including Effects From Different Storm Drivers, *J.*  
863 *Geophys. Res.*
- 864 Usanova, M. E., A. Drozdov, K. Orlova, I. R. Mann, Y. Shprits, M. T. Robertson, D. L.  
865 Turner, D. K. Milling, A. Kale, D. N. Baker, S. A. Thaller, G. D. Reeves, H. E. Spence,  
866 C. Kletzing, and J. Wygant (2014), Effect of EMIC waves on relativistic and ultrarelativis-  
867 tic electron populations: Ground-based and Van Allen Probes observations, *Geophys. Res.*  
868 *Lett.*, *41*, 1375–1381, doi:10.1002/2013GL059024.
- 869 Van Allen, J. A. (1981), Observations of high intensity radiation by satellites 1958 Alpha and  
870 1958 Gamma, in *Space Science Comes of Age: Perspectives in the History of the Space*  
871 *Sciences*, edited by P. A. Hanle, V. D. Chamberlain, and S. G. Brush, pp. 58–73.
- 872 Wang, C.-P., R. Thorne, T. Z. Liu, M. D. Hartinger, T. Nagai, V. Angelopoulos, J. R. Wygant,  
873 A. Breneman, C. Kletzing, G. D. Reeves, S. G. Claudepierre, and H. E. Spence (2017), A  
874 multispacecraft event study of Pc5 ultralow-frequency waves in the magnetosphere and  
875 their external drivers, *Journal of Geophysical Research (Space Physics)*, *122*, 5132–5147,  
876 doi:10.1002/2016JA023610.

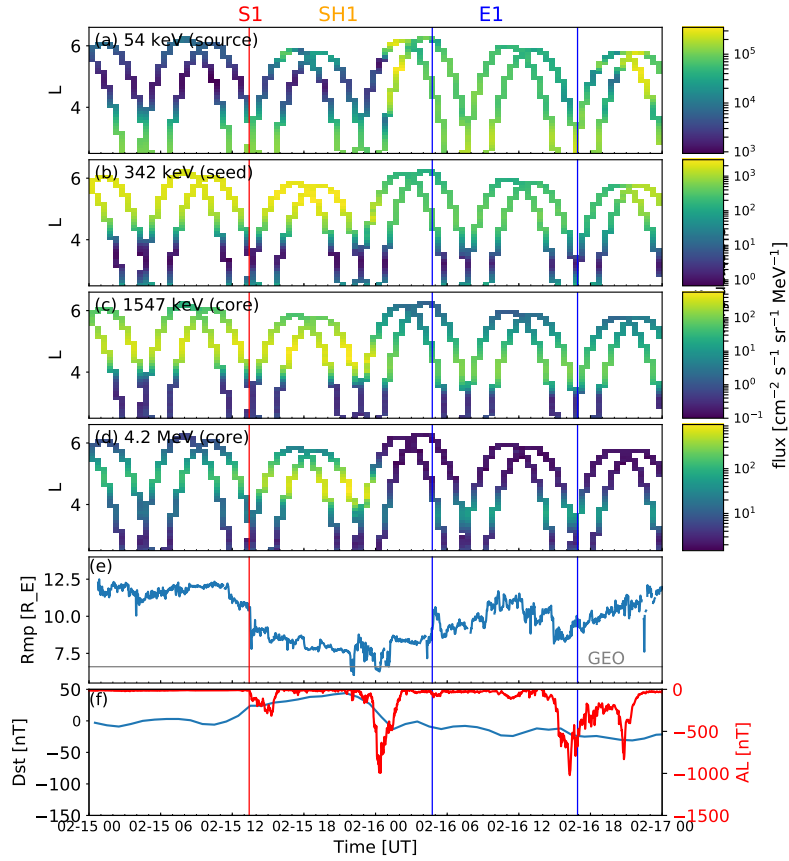
- 877 West, H. I., R. M. Buck, and J. R. Walton (1972), Shadowing of Electron Azimuthal-Drift  
878 Motions near the Noon Magnetopause, *Nature Physical Science*, *240*, 6–7, doi:10.1038/  
879 physci240006a0.
- 880 Xiao, F., S. Liu, X. Tao, Z. Su, Q. Zhou, C. Yang, Z. He, Y. He, Z. Gao, D. N. Baker, H. E.  
881 Spence, G. D. Reeves, H. O. Funsten, and J. B. Blake (2017), Generation of extremely low  
882 frequency chorus in Van Allen radiation belts, *Journal of Geophysical Research (Space*  
883 *Physics)*, *122*, 3201–3211, doi:10.1002/2016JA023561.
- 884 Zhang, J., I. G. Richardson, D. F. Webb, N. Gopalswamy, E. Huttunen, J. C. Kasper, N. V.  
885 Nitta, W. Poomvises, B. J. Thompson, C.-C. Wu, S. Yashiro, and A. N. Zhukov (2007),  
886 Solar and interplanetary sources of major geomagnetic storms ( $Dst \leq -100$  nT) during  
887 1996-2005, *Journal of Geophysical Research (Space Physics)*, *112*, A10102, doi:10.1029/  
888 2007JA012321.



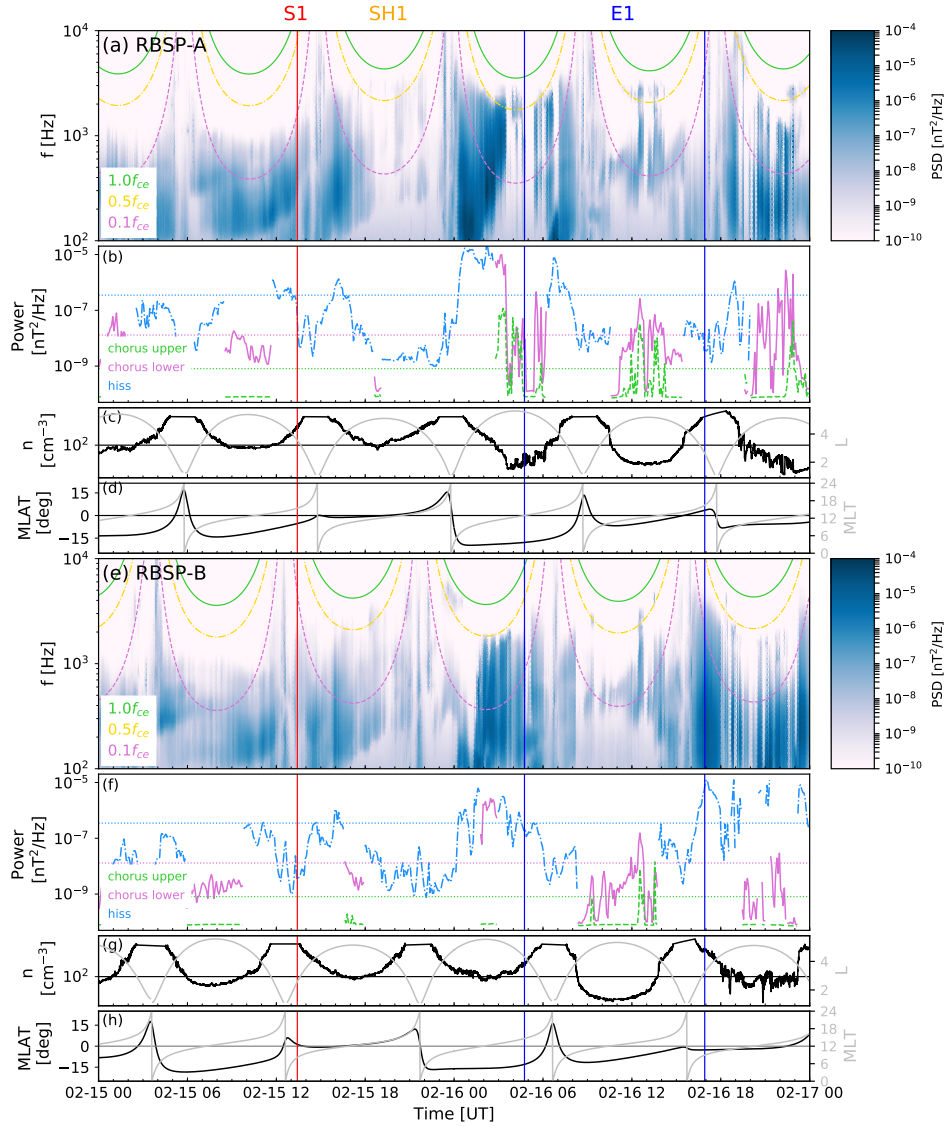
252 **Figure 1.** The panels show from top to bottom a) magnetic field magnitude, b) magnetic field north-south  
 253 component in the Geocentric Solar Magnetospheric (GSM) coordinate system, c) solar wind speed, d) solar  
 254 wind dynamic pressure (blue) and subsolar magnetopause position from the *Shue et al.* [1998] model (red),  
 255 e) AL index, f) Dst index (1-hour). The red vertical lines mark the shock, and the blue lines bound the ICME  
 256 intervals. The orange-shaded regions indicate the sheath intervals and the blue shaded-regions the ICME  
 257 intervals. S, E and SH stand for shock, ejecta and sheath.



258 **Figure 2.** The panels show: The electron fluxes of a) 54 keV (source), c) 342 keV (seed), e) 1547 keV  
 259 (core), and g) 4.2 MeV from Van Allen Probes MAGEIS (54, 342 and 1547-keV electrons) and REPT (4.2-  
 260 MeV electrons) instruments. The panels b), d), f) and h) show the maximum flux for each energies. The color  
 261 coding shows the L-value of the maximum flux. The Van Allen Probes data plots shows the data combined  
 262 from both A and B probes and is averaged over 6-hour time and 0.1 L-shell bins.

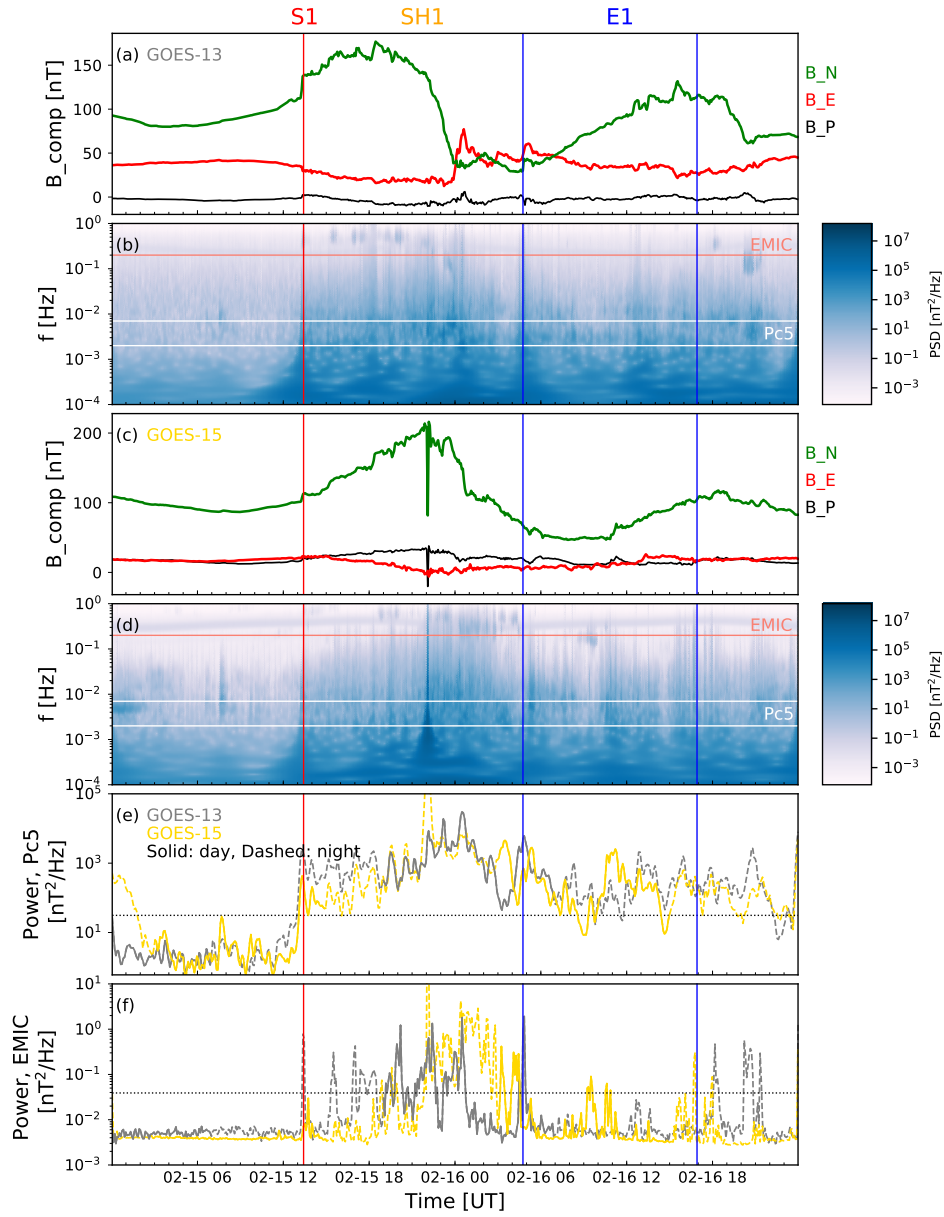


271 **Figure 3.** Zoom in to February 15–16, 2014 (Period 1). This interval includes the first shock (S1) and  
 272 the following sheath (S1) and ejecta (E1). The electron fluxes of a) 54 keV (source), b) 342 keV (seed), c)  
 273 1547 keV (core), and d) 4.2 MeV from Van Allen Probes using the 30 minute averages of MAGEIS (54, 342  
 274 and 1547-keV electrons) and REPT (4.2-MeV electrons) instruments data, e) subsolar magnetopause posi-  
 275 tion from the *Shue et al.* [1998] model, and f) Dst (blue) and AL (red) indices). The red vertical line shows  
 276 shock S1 and the blue vertical lines mark ejecta E1 interval.

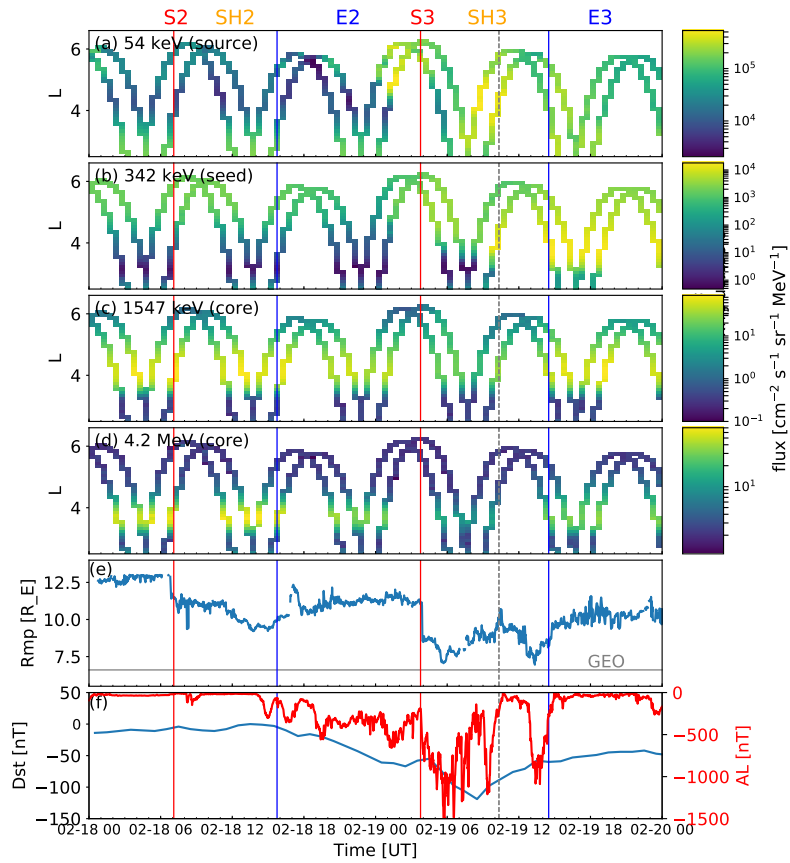


277 **Figure 4.** Chorus and hiss waves during February 15–16, 2014 (Period 1). The panels show: a) and e) the  
 278 magnetic spectral density, b) and f) the power in the lower (magenta) and upper (green) chorus bands when  
 279 the Van Allen Probes were outside the plasmasphere ( $n < 100 \text{ cm}^{-3}$ ) and hiss power (blue) when the Van  
 280 Allen Probes were inside the plasmasphere  $n > 100 \text{ cm}^{-3}$ ) and g)  $L$ -shell, and plasma density from Van Allen  
 281 Probes EMFISIS, and d) and h) MLT and MLAT. In panels a) and e) the green solid line represent  $f_{ce,eq}$ , yel-  
 282 low dash-dotted line  $0.5 f_{ce,eq}$ , and the magenta dashed line  $0.1 f_{ce,eq}$ . Inbound orbits are from the apogee to  
 283 perigee (duskside), and outbound orbits from perigee to apogee (dawnside). The horizontal lines in panels c)  
 284 and g) mark  $n = 100 \text{ cm}^{-3}$ . The horizontal magenta, green and blue lines in panels b) and f) show 10 times  
 285 the quiet time level for lower and upper chorus and hiss power (see Section 2 for details).

The red vertical line shows shock S1 and the blue vertical lines mark ejecta E1 interval.

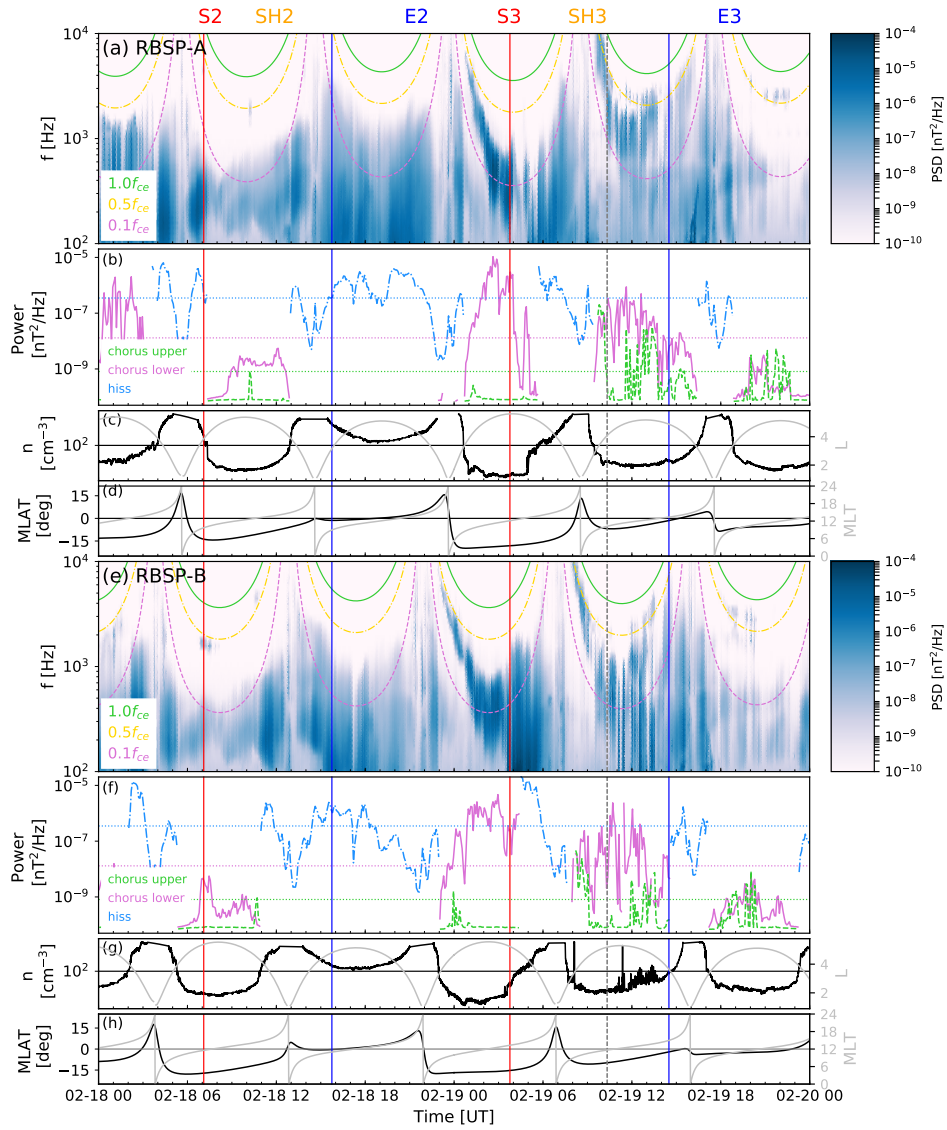


286 **Figure 5.** ULF waves during February 15-16, 2014 (Period 1) as observed by the geostationary GOES-13  
 287 and GOES-15 satellites. The panels show: a) and c) magnetic field components, b) and d) the wavelet power  
 288 spectra summed from all magnetic field components, and the power calculated at the e) Pc5 frequencies (2–10  
 289 minutes), and f) frequencies from 1 to 5 seconds (the 1 second being minimum possible time cadence) rep-  
 290 representing EMIC power. The gray curves show the power for GOES-13 and gold curves for GOES-15. The  
 291 dashed lines show the night time observations and solid lines day time observations. The horizontal lines in  
 292 panels e) and f) show 10 times the quiet-time level for ULF Pc5 and EMIC wave power (see text for details).  
 293 The red vertical line shows the shock S1 and the blue vertical lines mark the ejecta E1 interval.

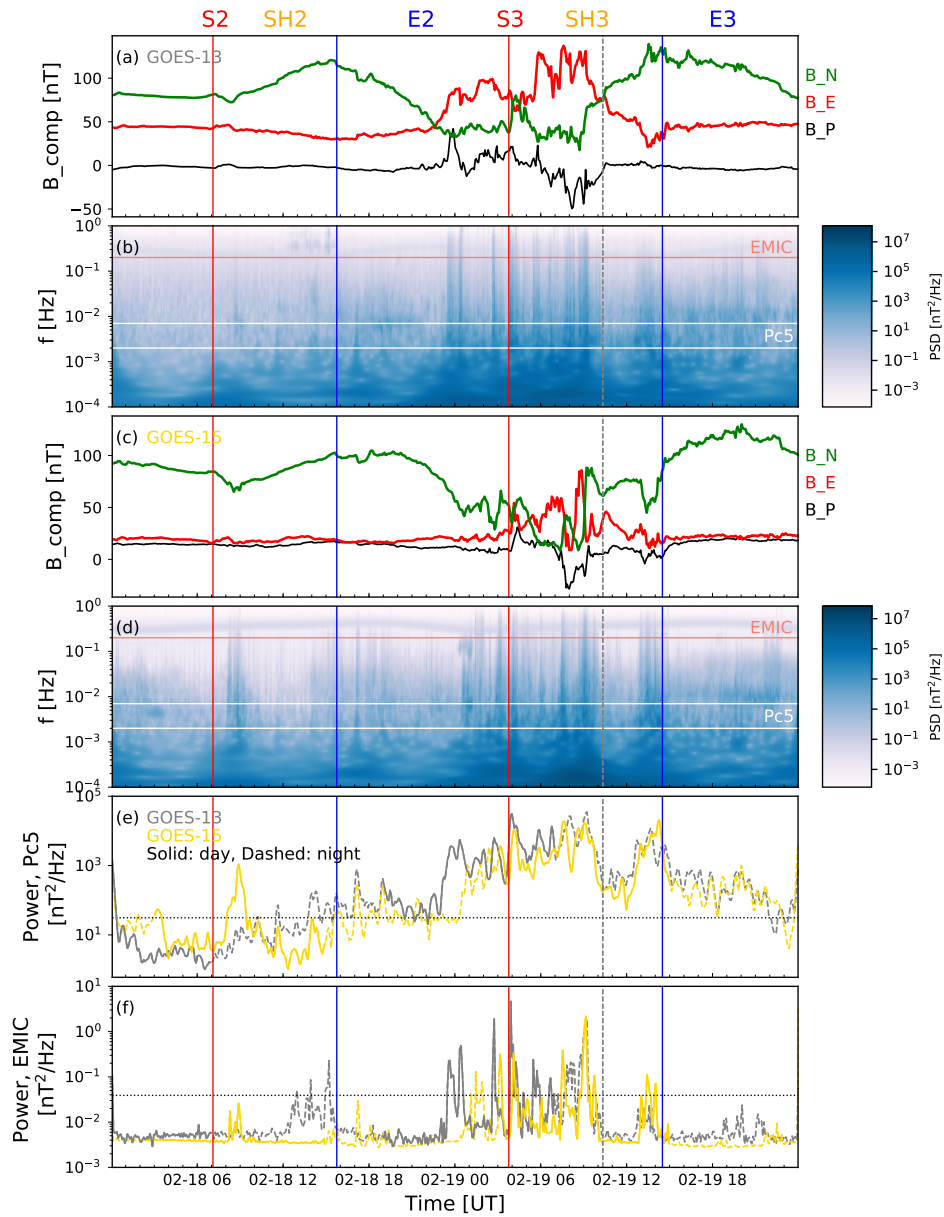


338 **Figure 6.** Zoom in to February 18–19, 2014 (Period 2). This interval includes second and third ICMEs,  
 339 including related shocks (S2 and S3), sheaths (SH2 and SH3), and ejecta (E2 and E3). The panels are same as  
 340 in 3. The red vertical lines show the shock S2 and S3, the first and second blue vertical lines show the ejecta  
 341 E2 and E3 leading edge times, and the dashed gray line the approximate end time of E2.

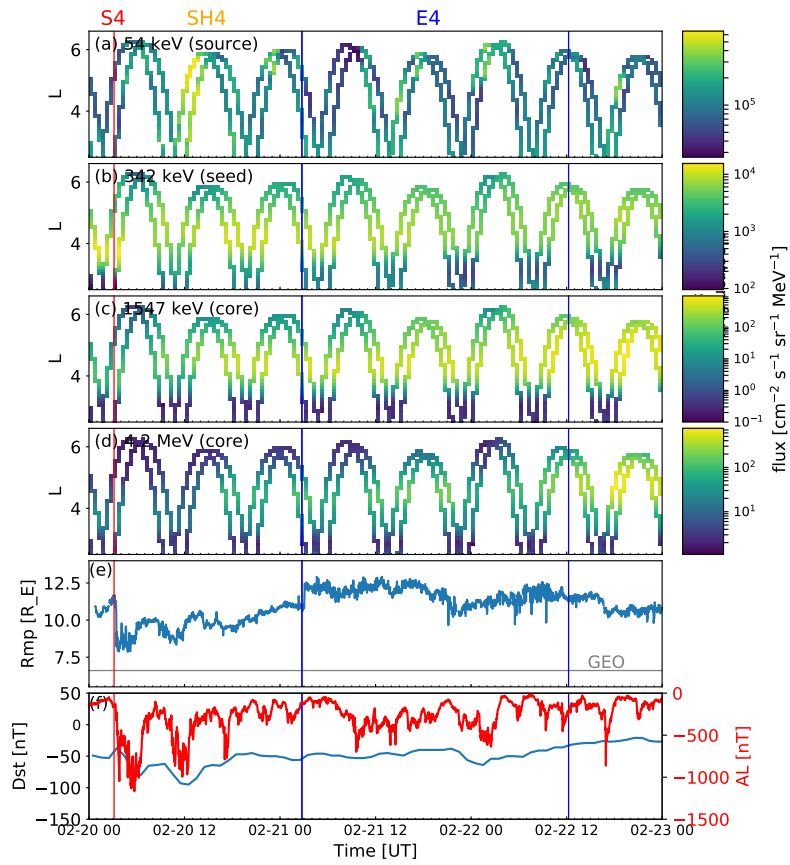




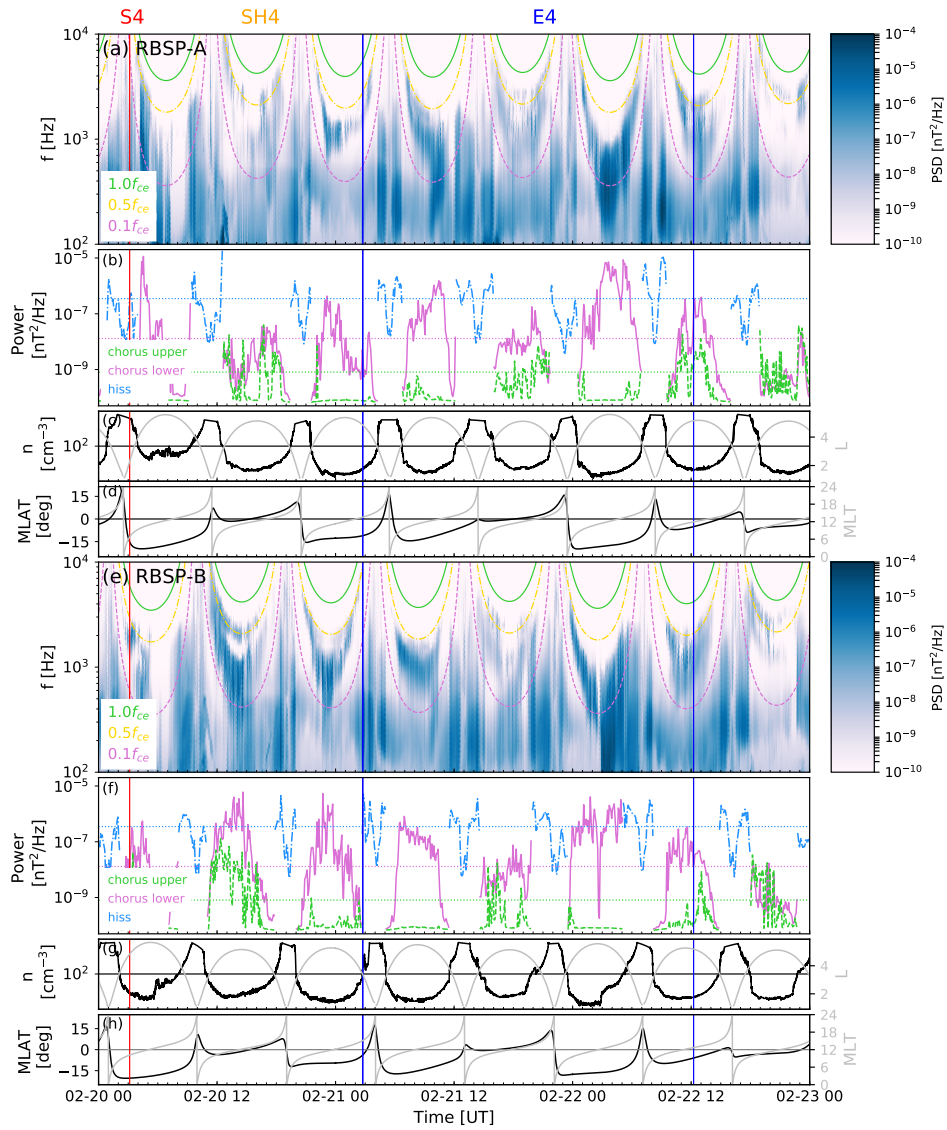
342 **Figure 7.** Chorus and hiss waves during February 18–19, 2014 (Period 2). The panels are same as in Figure  
 343 4. The red vertical lines show the shock S2 and S3, the first and second blue vertical lines show the ejecta E2  
 344 and E3 leading edge times, and the dashed gray line the approximate end time of E2.



345 **Figure 8.** ULF waves during February 18–19, 2014 (Period 2) as observed by the geostationary GOES-13  
 346 and GOES-15 satellites. The panels are same as in 5. The red vertical lines show the shock S2 and S3, the  
 347 first and second blue vertical lines show the ejecta E2 and E3 leading edge times, and the dashed gray line the  
 348 approximate end time of E2.



404 **Figure 9.** Zoom in to February 20-22, 2014 (Period 3). This interval includes fourth ICME, i.e., shock S4,  
 405 sheath SH4 and ejecta E4. The panels are same as in 3. The red vertical line shows the shock S4 and the blue  
 406 vertical line marks the ejecta E4.

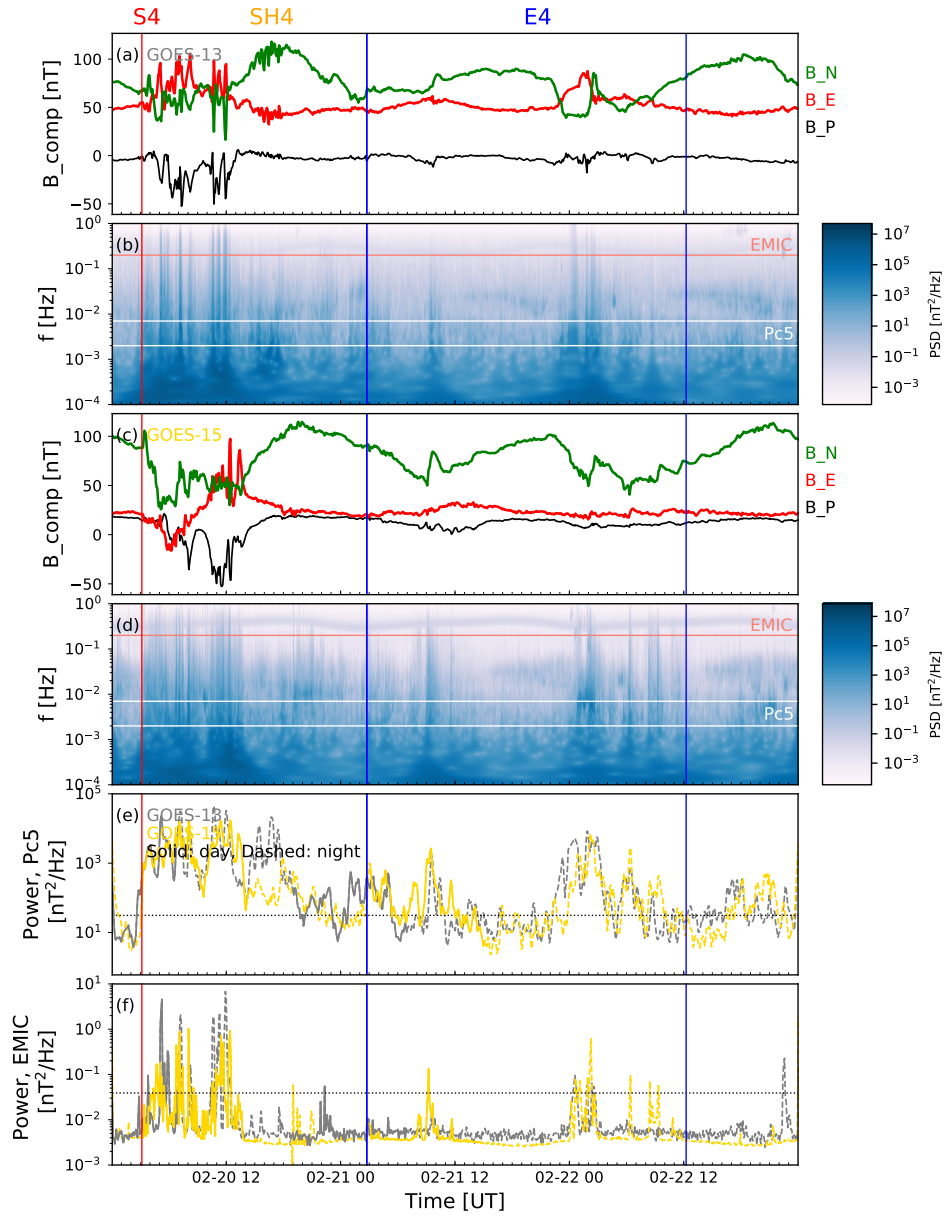


407

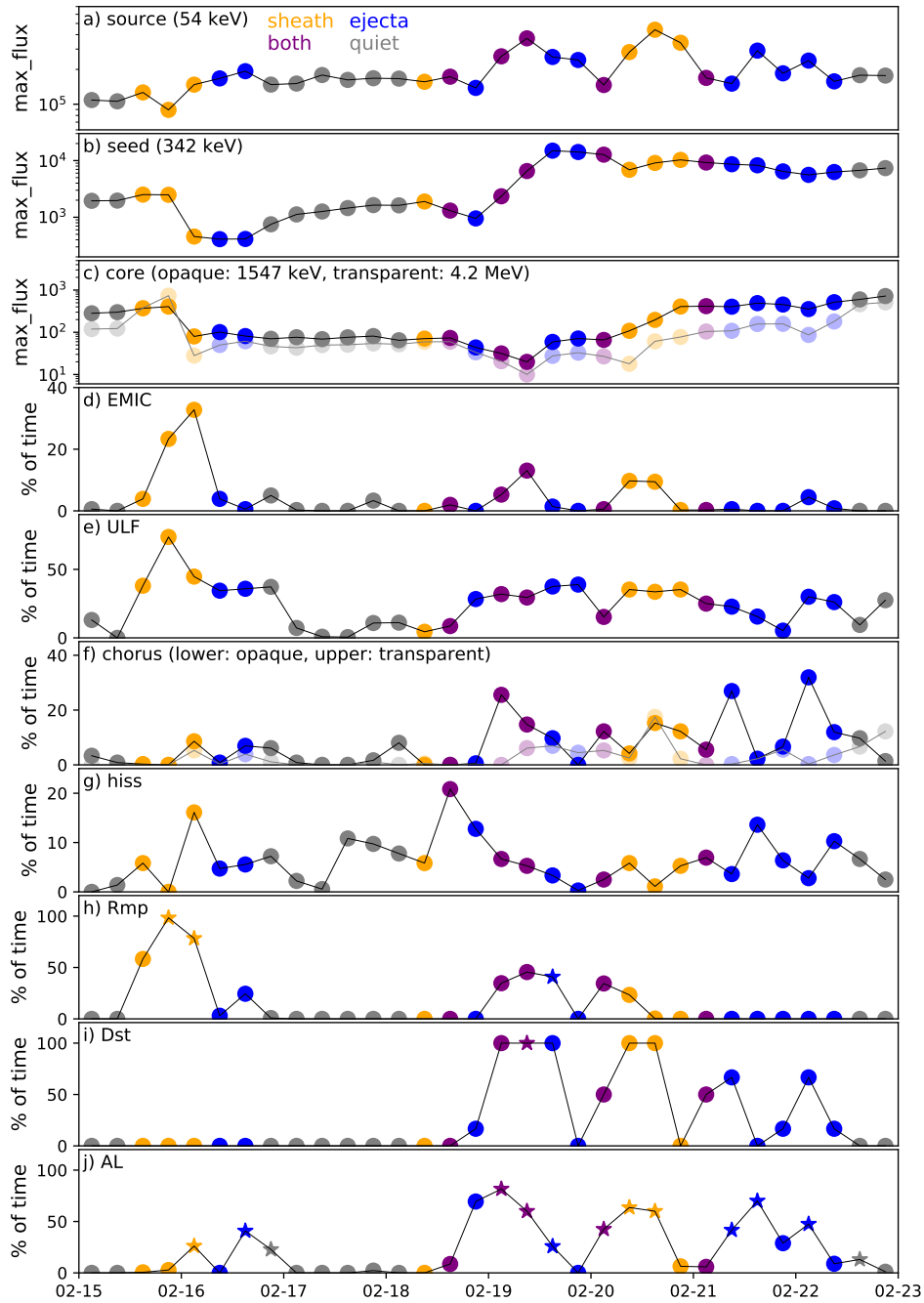
**Figure 10.** Chorus and hiss waves during February 20–22, 2014 (Period 3). The panels are same as in

408

Figure 4. The red vertical line shows the shock S4 and the blue vertical line marks the ejecta E4.



409 **Figure 11.** ULF waves during February 20–21, 2014 (Period 3) as observed by the geostationary GOES-13  
 410 and GOES-15 satellites. The panels are same as in 5. The red vertical line shows the shock S4 and the blue  
 411 vertical line marks the ejecta E4.



460 **Figure 12.** Overview of conditions during the studied interval for the same 6-hour blocks as in Figure 2.  
 461 The panels show from top to bottom: Maximum flux for a) source, b) seed, c) core populations (opaque: 1547  
 462 keV, transparent: 4.2 MeV). Units are  $\text{cm}^2 \text{ sr keV}^{-1}$ . The percentage of time during the 6-hour intervals  
 463 when ten times quiet time levels (see Table 1) were exceeded for d) EMIC, e) ULF Pc5, f) lower and upper  
 464 band, and g) hiss powers. The three bottom panels show the percentage of time with h) subsolar magne-  
 465 topause position  $R_{mp} < 9 R_E$ , i)  $Dst < -50 \text{ nT}$ , and j)  $AL < -300 \text{ nT}$ . The stars in panels h), i) and j) indicate  
 466 the periods when  $R_{mp} < 7 R_E$ ,  $Dst < -100 \text{ nT}$ ,  $AL < -600 \text{ nT}$ . The color-coding show the type of the solar  
 467 wind structure (gray: undisturbed solar wind, orange: sheath, blue: ejecta, purple: both).